NASA/TM—2002-212000

Management of Total Pressure Recovery, Distortion and High Cycle Fatigue in Compact Air Vehicle Inlets

Bernhard H. Anderson
Glenn Research Center, Cleveland, Ohio

Henry D. Baust
Wright-Patterson Air Force Base, Dayton, Ohio

Johan Agrell
Swedish Defence Research Agency, Bromma, Sweden

December 2002

The NASA STI Program Office . . . in Profile

Since its founding, NASA has been dedicated to the advancement of aeronautics and space science. The NASA Scientific and Technical Information (STI) Program Office plays a key part in helping NASA maintain this important role.

The NASA STI Program Office is operated by Langley Research Center, the Lead Center for NASA's scientific and technical information. The NASA STI Program Office provides access to the NASA STI Database, the largest collection of aeronautical and space science STI in the world. The Program Office is also NASA's institutional mechanism for disseminating the results of its research and development activities. These results are published by NASA in the NASA STI Report Series, which includes the following report types:

- TECHNICAL PUBLICATION. Reports of completed research or a major significant phase of research that present the results of NASA programs and include extensive data or theoretical analysis. Includes compilations of significant scientific and technical data and information deemed to be of continuing reference value. NASA's counterpart of peer-reviewed formal professional papers but has less stringent limitations on manuscript length and extent of graphic presentations.

- TECHNICAL MEMORANDUM. Scientific and technical findings that are preliminary or of specialized interest, e.g., quick release reports, working papers, and bibliographies that contain minimal annotation. Does not contain extensive analysis.

- CONTRACTOR REPORT. Scientific and technical findings by NASA-sponsored contractors and grantees.

- CONFERENCE PUBLICATION. Collected papers from scientific and technical conferences, symposia, seminars, or other meetings sponsored or cosponsored by NASA.

- SPECIAL PUBLICATION. Scientific, technical, or historical information from NASA programs, projects, and missions, often concerned with subjects having substantial public interest.

- TECHNICAL TRANSLATION. English-language translations of foreign scientific and technical material pertinent to NASA's mission.

Specialized services that complement the STI Program Office's diverse offerings include creating custom thesauri, building customized databases, organizing and publishing research results . . . even providing videos.

For more information about the NASA STI Program Office, see the following:

- Access the NASA STI Program Home Page at ***http://www.sti.nasa.gov***

- E-mail your question via the Internet to help@sti.nasa.gov

- Fax your question to the NASA Access Help Desk at 301–621–0134

- Telephone the NASA Access Help Desk at 301–621–0390

- Write to:
  NASA Access Help Desk
  NASA Center for AeroSpace Information
  7121 Standard Drive
  Hanover, MD 21076

NASA/TM—2002-212000

Management of Total Pressure Recovery, Distortion and High Cycle Fatigue in Compact Air Vehicle Inlets

Bernhard H. Anderson
Glenn Research Center, Cleveland, Ohio

Henry D. Baust
Wright-Patterson Air Force Base, Dayton, Ohio

Johan Agrell
Swedish Defence Research Agency, Bromma, Sweden

National Aeronautics and
Space Administration

Glenn Research Center

December 2002

The Aerospace Propulsion and Power Program at
NASA Glenn Research Center sponsored this work.

Available from

NASA Center for Aerospace Information
7121 Standard Drive
Hanover, MD 21076

National Technical Information Service
5285 Port Royal Road
Springfield, VA 22100

Available electronically at http://gltrs.grc.nasa.gov

MANAGEMENT OF TOTAL PRESSURE RECOVERY, DISTORTION AND HIGH CYCLE FATIGUE IN COMPACT AIR VEHICLE INLETS

Bernhard H. Anderson
National Aeronautics and Space Administration
Glenn Research Center
Cleveland, Ohio

Henry D. Baust
Wright-Patterson Air Force Base
Dayton, Ohio

Johan Agrell
Swedish Defence Research Agency
Bromma, Sweden

ABSTRACT

It is the purpose of this study to demonstrate the viability and economy of *Response Surface Methods* (RSM) and *Robust Optimization Concepts* (ROC) to arrive at micro-secondary flow control installation designs that maintain optimal inlet performance over a range of the mission variables. These statistical design concepts were used to investigate the robustness properties of "low unit strength" micro-effector installations. "Low unit strength" micro-effectors are micro-vanes set at very low angles-of-incidence with very long chord lengths. They were designed to influence the near wall inlet flow over an extended streamwise distance, and their advantage lies in low total pressure loss and high effectiveness in managing engine face distortion.

To illustrate the potential of economical robust design methodology, three different mission strategies were considered for the subject inlet, namely (1) Maximum Performance, (2) Maximum Engine Stability, and (3) Maximum High Cycle Fatigue Life Expectancy. The Maximum Performance mission minimized the inlet total pressure losses, the Maximum Engine Stability mission minimized the engine face distortion (DC60), while the Maximum HCF Life Expectancy mission minimized the mean of the first five Fourier harmonic amplitudes, i.e. "collectively" reduced all the harmonic 1/2-amplitudes of engine face distortion. Each of the mission strategies was subject to a low engine face distortion constraint, i.e. DC60 $\leq$ 0.10, which is a level acceptable for commercial engines, and to place a constraint on each individual Fourier harmonic amplitude of Fk/2 $\leq$ 0.015. For each of these missions strategies, an "Optimal Robust" (open loop control) and an "Optimal Adaptive" (closed loop control), installation were designed over an inlet throat Mach number range from 0.30 to 0.70, and angle-of-incidence range from 0.0^{o} to 20.0^{o}. The "Optimal Robust" installation used economical Robust Design methodology to arrive at a single design, which operated over the entire throat Mach number and angle-of-incident range (open loop control). The "Optimal Adaptive" installation optimized all the design parameters at each throat Mach number and angle-of-incidence. Thus the "Optimal Adaptive" installation would require a closed loop control system to sense a proper signal for each effector and modify that effector device, whether mechanical or fluidic, for optimal inlet performance. In general, the performance differences between the "Optimal Adaptive" and "Optimal Robust" installation

designs were found to be marginal. This suggests, that "Optimal Robust" opened loop installation designs can be very competitive with "Optimal Adaptive" closed loop designs.

Effective inlet flow control management of engine face distortion was achieved by reducing the unit strength of the micro-vane effector and allowing the installation design to influence the inlet flow over an extended streamwise distance. With this combination, the total pressure losses associated with micro-vane effectors became very small, and a large overall performance gain was achieved. In addition, this study demonstrated that optimal "low unit strength" micro-effector installation designs exhibited the same robustness properties as optimal "high unit strength" micro-effector installation but without the large total pressure loss. The design strategy of replacing "high unit strength" micro-effectors with "low unit strength" micro-effectors which influence the flow over an extended streamwise distance was therefore found to be very effective.

INTRODUCTION

The current development strategy for combat air-vehicles is directed towards reduction in the Life-Cycle Cost (LCC) with little or no compromise to air-vehicle performance and survivability. This strategy has been extended to the aircraft component level, in particular, the engine inlet diffuser system. One method to reduce inlet system LCC is to reduce its structural weight and volume. Consequently, advanced combat inlet configurations are being made more compact (or shorter) to achieve weight and volume (and LCC) reduction. However, compact S-duct diffusers (see Figures (1) and (2)) are characterized by high distortion and low pressure recovery, which are produced by extreme wall curvature and strong secondary flow gradients. These characteristics are further aggravated by maneuvering conditions. Since survivability rather than aerodynamic performance often drives the inlet design, it is expected that the flow quality entering the turbine engine will present an additional challenging environment for both fan/compressor surge margin and aeromechanical vibration. Interest in High Cycle Fatigue (HCF) research by the US aerospace community has been spurred by discrepancies between the expected durability of engine components compared to that actually experienced in the field. Recognizing that inlet distortion is a forcing function for vibration in the fan components, methods for increasing HCF Life Expectancy can be combined with techniques for inlet recovery and engine face distortion management. Therefore, to enable acceptable performance levels in such advanced, compact inlet diffuser configurations, micro-scale secondary flow control (MSFC) methods are being developed to manage the recovery, distortion, and HCF aspects of distortion.[1]-[2]

One of the most difficult tasks in the design of a MSFC installation for optimal inlet operation is arriving at the geometric placement, arrangement, number, size and orientation of the effector devices within the inlet duct to achieve optimal performance.These effector devices can be either mechanical or fluidic.This task is complicated not only by the large number of possible design variables available to the aerodynamicist but also by the number of decision parameters that are brought into the design process. By including the HCF effects in the inlet design process, the aerodynamicist has a total of seven individual response variables that measure various aspects of inlet performance. These include the inlet total pressure recovery, the inlet total pressure recovery distortion at the engine face and the first five Fourier harmonic 1/2-amplitudes contained in the engine face distortion pattern. Each of these responses must be maximized, minimized, constrained or unconstrained while searching for the optimal combination of primary design variable values that satisfy the mission requirements. The design task is further complicated by the exist-

ence of hard-to-control factors that affect inlet performance, i.e. the mission variables. The mission variables that cause the off-design penalty are, for example, inlet throat Mach number (engine corrected weight flow), angle-of-incidence and angle-of-yaw. While the aerodynamicist does not know how the pilot is ultimately going to fly the aircraft, it is known how the mission variables affect inlet performance under wind tunnel conditions. Traditionally, tolerance or robustness to the mission variables was accomplished only after the parameter design was completed, usually by accepting whatever off-design performance was delivered by the newly designed inlet system. Numerical optimization procedures that have been successful with some aerodynamics problems give little assistance to designing robust inlets since they are point-design procedures, usually with only one decision parameter. However, there is a branch of statistical Design-of-Experiments (DOE) methodology which integrates both traditional *Response Surface Methods* (RSM) and *Robust Optimization Concepts* (ROC) into a single optimization procedure. It presents new potential for further reduction of *total quality cost* over the traditional design approach.

Taguchi[3] coined the term Robust Parameter Design to describe an approach to industrial problem solving whereby the product variation is reduced by choosing levels of the control factors (design parameters) that make the product insensitive to the changes in the noise factors that represent sources of variations. These noise factors in industrial design are often the environmental variables such as temperature and humidity, properties of the material, and product aging. In some applications, the factors measure how the consumer uses or handles the product. In the aerodynamic design of inlet systems, there is an analogous situation to the industrial design problem. As mentioned above, the design of inlet systems is usually accomplished at the cruise condition (the on-design condition) while variations from the cruise condition are considered as an off-design penalty. The variables that cause the off-design penalty are the mission variables, such as the inlet throat Mach number (engine corrected weight flow), angle-of-incidence and angle-of-yaw. Because the mission variables cause variation from on-design performance, they can be identified with the noise factors or environmental variables in the analogous industrial design problem. Likewise, how the pilot flies the aircraft can be identified with how the consumer uses or handles the product. In the industrial problem, researchers must be able to control the environmental variables in a laboratory environment, even though they cannot be controlled at the production level or in the field. Likewise, the aerodynamic researcher can indeed control the mission variables in the wind tunnel environment, however these variables cannot be controlled in flight (in the field). By making the analogy between the industrial design problem and the aerodynamic design problem, *Robust Parameter Design* methods developed for industrial problem solving can be adapted to the design of inlet systems, and in particular, design of micro-scale secondary flow control installations for such inlet systems.

Much has been written and said about the contribution of Genichi Taguchi to the vastly important area of *Product Quality Enhancement*. However, much controversy surrounds Taguchi's methodology among statisticians. Many statisticians have pointed out the apparent flaws in the Taguchi approach. However, it suffices to say the importance of Taguchi's contributions lies in the idea that process or product sensitivity to its environment can be incorporated into the optimal statistical Design-of-Experiment and subsequent analysis of data. To the aerodynamicist, it represents a quantum leap in the area of aerodynamic design. For the first time, the mission variables can be directly introduced into the aerodynamic design processes. The inlet system can now be designed to operate with optimal performance over a range of specified mission variables. Rigorous application of Taguchi's Robust Parameter Design method may not be optimal in the

design of micro-scale secondary flow installations for inlet systems because it can mask information vital to the aerodynamicist. However, the important aspects surrounding Taguchi's approach to *Robust Parameter Design* have been incorporated into an alternate approach, i.e. adapted to the inlet design problem by Anderson and Keller.[4] The approach taken by Anderson and Keller was a combined DOE format in which the factor (design) variables and the environmental (mission) variables were contained in the same DOE. This approached, called the lower order combined DOE format, led to a very viable and economical methodology to explore the concept of robust inlet design (Anderson and Keller[5]-[6]). The concept of robust inlet design means that the inlet mission variables are brought directly into the installation design process, and insensitivity or robustness to the mission variables becomes a design objective. More importantly, the combined DOE format allows for conceptual studies to be made of the inlet-engine control system, which take advantage of the inherent robustness properties that have been built into the installation design by *Response Surface Methods* and *Robust Optimization Concepts*. It is the purpose of this report to expand the concept of inlet robust installation design to cover both the inlet throat Mach number and angle-of-incidence mission variable range and to explore the robustness properties of "low unit strength" micro-vane effector installation designs which exhibit very low total pressure loss and high effectiveness in managing engine face distortion.

To illustrate the potential of *Response Surface Methods* and *Robust Optimization Concepts* to provide open loop installation designs that exhibit optimal inlet performance over an extended mission variable range, three different mission strategies were considered for the subject inlet, namely (1) Maximum Performance, (2) Maximum Engine Stability, and (3) Maximum HCF Life Expectancy. The Maximum Performance mission minimized the inlet total pressure losses, the Maximum Engine Stability mission minimized the engine face distortion, while the Maximum HCF Life Expectancy mission minimized the mean of the first five Fourier harmonic amplitudes, i.e. "collectively" reduced all the harmonic 1/2-amplitudes of engine face distortion. Each of the mission strategies was subject to a low engine face distortion constraint, i.e. $DC60 \leq 0.10$, which is a level acceptable for commercial engines, and a constraint on each individual Fourier harmonic amplitudes of $Fk/2 \leq 0.015$. For each of three mission strategies, i.e Maximum Performance, Maximum Engine Stability, and Maximum HCF Life Expectancy mission, an "Optimal Robust" (open loop control) and an "Optimal Adaptive" (closed loop control) installation were designed to operate over an inlet throat Mach number range from 0.30 to 0.70, and angle-of-incidence, i.e. α-range from 0.0^{o} to 20.0^{o}. The "Optimal Robust" installation arrived at a single MSFC installation which operated optimally over the entire throat Mach number and angle-of-incidence range (open loop control). The "Optimal Adaptive" installation optimized all the design parameters at each throat Mach number and angle-of-incidence. Thus the "Optimal Adaptive" installation would require a closed loop control system to sense a proper signal for each effector and modify that effector device, whether mechanical or fluidic, for optimal inlet performance. For each of the three mission strategies, i.e. Maximum Performance, Maximum Engine Stability, and Maximum HCF Life Expectancy, two approaches to secondary flow control installation design, i.e. "Optimal Robust" installation design and Optimal Adaptive" installation design, were compared for the simultaneous management of inlet total pressure recovery, engine face distortion, and the first five Fourier harmonic 1/2-amplitudes of distortion. The throat Mach number and angle-of incidence range were the Taguchi noise or environmental variables over which each optimal installation had to be robust.

NOMENCLATURE

AIP	Aerodynamic Interface Plane
c	Effector Chord Length
CCF	Central Composite Face-Centered
CFD	Computational Fluid Dynamics
D	Engine Face Diameter
DC60	Circumferential Distortion Descriptor
DOE	Design of Experiments
h	Effector Blade Height
HCF	High Cycle Fatigue
Fk/2	k^{th} Fourier Harmonic 1/2-Amplitude
FM/2	Mean Fourier Harmonic 1/2-Amplitude
L	Inlet Diffuser Length
LCC	Life Cycle Costs
MSFC	Micro-Scale Secondary Flow Control
Mt	Inlet Throat Mach Number
n	Number of Effector Vanes per Band
PFAVE	Average Inlet Total Pressure at AIP
PAVCRIT	Minimum Total Pressure over Critical Sector Angle at AIP
QAVE	Average Dynamic Pressure at AIP
R	Inlet Radius
R_{cl}	Centerline Radius
R_{ef}	Engine Face Radius
R_{thr}	Inlet Throat Radius
ROC	Robust Optimization Concepts
Re	Reynold Number per ft.
RSM	Response Surface Methodology
S	Standard Deviation
S_{clock}	Standard Deviation over the Rake Clocking Angles
UAV	Unmanned Air Vehicle
UCAV	Unmanned Combact Air Vehicle
X_{cl}	Axial Distance Along the Duct Centerline
Y_A	Upper 95% Confidence Interval Predicted by DOE Analysis
Y_{CFD}	Response Predicted by CFD Analysis
Y_{DOE}	Response Predicted by DOE Analysis
$Y_{i,j}$	Generalized Response Variable
$Y_{M,\alpha}$	Generalized Response Variable Summed over Mt and α
Z_{cl}	Centerline Offset Displacement
α	Inlet Angle-of-Incidence
β	Effector Vane Angle-of-Incidence
ΔZ_{cl}	Inlet Centerline Offset
γ	Inlet Angle-of-Yaw

RESULTS AND DISCUSSION

Baseline Flow in the Redesigned M2129 Inlet S-Duct

The redsigned M2129 inlet S-duct used in this study was considered similar to the original DERA/M2129 inlet S-duct defined by AGARD FDP Working Group 13 Test Case 3,[7] using Lip No. 3 and Forward Extension No. 2. This inlet design was first proposed by Willmer, Smith and Goldsmith,[8] and has been used extensively in the US and UK to explore inlet flow control installation design. The centerline for the redesigned M2129 inlet is given by the equation

$$Z_{cl} = -\Delta Z_{cl}\left(1 - \cos\left(\pi \cdot \frac{X_{cl}}{L}\right)\right) \qquad (1)$$

the radius distribution measured normal to the inlet centerline is given by the expression

$$\left(\frac{R_{cl} - R_{thr}}{R_{ef} - R_{thr}}\right) = 3\left(1 - \frac{X_{cl}}{L}\right)^4 - 4\left(1 - \frac{X_{cl}}{L}\right)^3 + 1 \qquad (2)$$

where R_{thr} = 2.5355 inches, R_{ef} = 3.0 inches, L = 15.0 inches, and ΔZ_{cl} = 5.401 inches. The redesign of the M2129 inlet was such that the new inlet matches the static pressure gradients normally found in typical UAV or UCAV designs. Therefore, the new inlet is more compact than the original M2129 inlet S-duct. As a consequence, supersonic flow will develop in this inlet when the inlet throat Mach number increases much above 0.70. The geometry and grid structure for the resigned M2129 inlet S-duct is shown in Figure (1). The computational grid for the baseline solutions was a single block composed of 61x91x49 grid points in a half cylindrical grid topology.

A set of cases was run to characterize the performance in the baseline inlet S-duct over a range of throat Mach numbers from 0.30 to 0.70 and angles-of-incidence from 0.0^o to 20.0^o. The definition of the baseline cases are presented in Table (1) and were organized as a full factorial array with two factors at three levels each, i.e. 3^2 cases. Each of the 9 cases in Table (1) were run with a Reynolds-averaged Navier-Stokes code.[10] The baseline inlet performance results are presented in Table (2) and include the inlet total pressure recovery (PFAVE), the engine face distortion (DC60), and the first five Fourier harmonic 1/2-amplitudes of engine face distortion (Fk/2). To introduce an angle-of-incidence (α-disturbance) into the flow analysis, the condition was imposed that the initial station have an angle-of-incidence component that approximated the measured angle-of-incidence flow field[11]. Even though introducing an α-disturbance into the flow field was not rigorous, it provided a remarkably good approximation in comparison to the experimental flow field. The data reduction methodology for the total pressure recovery, engine face distortion and Fourier harmonic 1/2-amplitudes appear in the section entitled Harmonic Analysis of Distortion.

The inlet was designed such that at 0.70 throat Mach number and 20.0° angle of incidence the Mach number in the vicinity of the inlet shoulder was just below supersonic conditions. Thus, if either the inlet throat Mach number increases much above 0.70 or the inlet angle-of-incidence increases beyond 20.0°, shock waves will form in the vicinity of the inlet shoulder which will induce massive flow separation extending upstream of the inlet throat. Over the range of throat Mach numbers from 0.30 to 0.70 and inlet angles-of-incidence from 0.0° to 20.0°, the inlet was separated. The degree of flow separation, i.e. vortex liftoff, is shown in Figure (2). This type of 3D flow separation results in severe total pressure losses and engine face distortion. In addition, it may also have very severe consequences with regard to aeromechanical vibration. The engine face total pressure recovery contours over the range of conditions presented in Table (1) are shown in Figure (3). Although the baseline flow for the redesigned M2129 inlet S-duct indicated vortex liftoff (flow separation) over the entire mission range defined by Table (1), there is considerable variation in distortion patterns shown in Figure (3). To augment this visual summary, the baseline inlet performance is presented in Figures (4) through Figure (9) in terms of the inlet total pressure recovery (PFAVE), engine face distortion (DC60), and the first five Fourier harmonic 1/2-amplitudes of engine face distortion (F1/2, F2/2, F3/2, F4/2, F5/2), and the mean of the first five Fourier harmonic 1/2-amplitudes (FM/2). Figures (4), (6) and (8) present the effect of inlet throat Mach number at 0.0° inlet angle-of-incidence on recovery, distortion, and Fourier harmonic 1/2-amplitudes of distortion, while Figures (5), (7) and (9) illustrate the effect of inlet angle-of-incidence on the same inlet metrics at an inlet throat Mach number of 0.70. The large variation in inlet performance is evident from these figures. Particularly revealing is the very high Fourier harmonic 1/2-amplitudes of distortion that can arise at angle-of-incidence conditions. See Figure (9).

Inlet Flow Control Design Approach

In the secondary flow control concept, micro-scale actuation is used as an approach called "secondary flow control" to alter the inlet S-duct inherent secondary flow with the goal of simultaneously improving the critical system level performance metrics of total pressure recovery, engine face distortion, and HCF characteristics. In studying the influence of micro-vane chord length[1] on inlet performance, it was determined that this factor was very important parameter in reducing engine face distortion as well as managing the harmonic content of engine face distortion. While there appear to be limits on the total number and strength of the individual effector units[1] in managing engine face distortion, there appear to be no such limits on micro-vane chord length. By installing multiple bands of micro-effector units, the chord length can be effectively increased,[5] and engine face distortion managed. However, this improvement in engine face distortion comes at the expense of total pressure recovery. In order to overcome the dimensional limit of chord length, the micro-vane angle of incidence can be greatly reduced while compensating for loss of unit strength by increasing the length of the micro-vane effector units. Hence effective inlet flow control management of engine face distortion can be achieved by reducing the unit strength of the vane effector and allowing the installation design to influence the inlet flow over a longer streamwise distance. With this combination, the total pressure losses associated with micro-vane effectors become very small, and a large overall performance gain achieved.

The micro-vane installations described in the first paragraph function by inducing a weak set of vortices in a cascade type arrangement within a very thin layer adjacent to the inlet walls. The weak set of vortices in this thin layer quickly merged to form a secondary flow field which suppressed the development of the vortex pair that forms in the diffuser, see Figures (2) and (3). This in turn, substantially reduced engine face distortion. It has been demonstrated that high unit strength micro-vane effectors with vane heights of 2.0 mm, chord length of 16.0 mm and a vane angle-of-incidence of 24.0^{o} manage the inlet flow very effectively at a throat Mach number of 0.70 and over a range of inlet angles-of-incidence from 0.0^{o} to 20.0^{o}. However, these high unit strength installation designs exhibited high total pressure loss. In other words, open loop installation designs using high unit strength micro-vane effectors were "Optimal Robust" over a range of inlet angles-of-incidence and differ only marginally in performance from "Optimal Adaptive" close loop installation designs.[4] However, the performance penalty paid for high unit strength "Optimal Robust" installation designs was high total pressure loss. In this study, low unit strength micro-vane effectors which have low total pressure loss will be examined to determine whether they exhibit the same robustness properties as high unit strength effectors. However, in this study, the "Optimal Robust" low unit strength micro-vane effector installation designs will be established over an expanded mission variable range, i.e. throat Mach numbers from 0.30 to 0.70 and inlet angles-of-incidence from 0.0^{o} to 20.0^{o}.

Inlet Flow Control Installation Design

To manage the flow in the redesigned M2129 inlet S-duct, a single band installation arrangement of micro-scale effectors was placed in the upstream section near the inlet throat. See Figures (10) and (11). These micro-scale effectors were micro-vanes, the largest height being about the average height of the momentum layer just downstream of the inlet throat or about 2.0 mm. The purpose of these micro-vanes was to create a set of co-rotating vortices that would quickly merge to form a thin layer of secondary flow that will counter the formation of the passage vortex pair. Since the height of the vane effectors were limited to 2.0 mm, a single-band arrangement of micro-vanes set at 5.0^{o} angle-of-incidence was chosen to investigate the enhancing effect of increasing the vane chord length on distortion management, i.e. allowing the installation design to influence the inlet flow over an extended streamwise distance for a design advantage

The DOE approach followed directly from the objectives previously stated and was reflected in the layout of the design factors listed in Table (3). The factor variables were the number of vane effector units (n), the micro-vane effector height (h), the micro-vane chord length (c), the inlet throat Mach number (Mt), and the inlet angle-of-incidence (α). Strictly speaking, the inlet throat Mach number and angle-of-incidence are mission variables and, therefore, the noise factors that belonged with the environmental variables, i.e. the outer array in a traditional Taguchi-style *Robust Parameter Design*. However, in this study, the throat Mach number and inlet angle-of-incidence were combined into the statistical DOE matrix with the control factors. This is called a combined DOE matrix array, which allowed greater economy than the traditional Taguchi approach[3]. The robust nature of the throat Mach number and inlet angle-of-incidence was investigated during the analysis phase of the data. Table (4) shows the variables that were held constant during this study. They include the effector vane thickness (t), the geometric angle-of-incidence of the micro vanes (β), the inlet operating total pressure (Pt) and temperature (Tt), and the inlet

angle-of-yaw (γ). Table (5) displays the response variables for this study. They include the inlet total pressure recovery (PFAVE), the engine face distortion (DC60), and the first five Fourier harmonic 1/2-amplitudes of engine face distortion (F1/2, F2/2, F3/2, F4/2, and F5/2).

The DOE strategy selected was a Central Composite Face-Centered (CCF) DOE. This strategy resulted in 27 unique CFD experimental cases that are shown in Table (6). This DOE construct is called a combined array format because it contains both the factor (design) variables and the environmental (mission) variables. Notice that these DOE cases covered a substantial range of possible flow situations over a wide range of throat Mach numbers from 0.30 to 0.70, and angles-of-incidences from 0.0^{o} to 20.0^{o}. This particular DOE, like most DOE strategies, varied more than one factor at a time. Further, this layout of 27 cases permitted the estimation of both linear and curvilinear effects as well as two-factor interactive or synergistic effects among the DOE factors. This CCF DOE strategy is superior to the traditional approach where only changing one variable at a time does not permit the estimation of the two-factor interactions. It is also more economical at 27 runs than a full factorial approach where the number of experiments would be 3^5 or 243 separate CFD cases. It is also more economical than a comparable Taguchi approach requiring 15 x 3 = 45 runs.

A graphical representation of the Central Composite Face-Centered DOE used in the study is presented in Figure (12). The DOE cases are represented in this figure by the circular symbols, where the symbol locations on the cube signify its factor value. This DOE is called a composite DOE because the organization of cases is composed of a fractional factorial part and a quadratic part. The fractional factorial part of the DOE is composed of one-half of the 2^5 possible cases, i.e. 32 possible factorial cases, which are represented by the eight corner locations in each of the four corner-cubes in Figure (12). Because only half the number of possible factorial cases are actually used in this DOE format (circular symbols), the layout is called a 1/2-fractional of the full factorial and is composed of 2^{5-1} cases, or 16 separate CFD runs. The remaining cases in Figure (12) are the quadratic part of the DOE. The quadratic cases allow for the evaluation of the curvilinear effects. All together, there are a total of 27 cases in a Central Composite Face-Centered DOE with five factor variables. Notice the balanced layout of cases in Figure (12). The factor variables are represented by the axes of the individual cubes, while the environmental variables are represented by the different cubes. This layout of cases represents the smallest number of CCF DOE cases that allows for the evaluation of linear and curvilinear effects as well as all two-factor interactive or synergistic effects.

Each of the 27 cases in Table (6) was run with a Reynolds-averaged Navier-Stokes code[10] that allowed for numerical simulation of micro-vane effectors without the need to physically embed the vane effectors within the CFD grid structure. However, for the present study the individual vanes were incorporated into the half cylindrical grid structure. These micro-vanes all had a thickness of 0.138 mm. See Table (4). The computational grid surrounding was developed such that it reasonably resolved the boundary layer development on both the suction and pressure surfaces of each micro-vane in the installation. Because wall functions were used in the calculations, the grid resolution for the individual micro-vanes was simplified. However, the boundary layer along the micro-vane edges was assumed to be negligible, and therefore not resolved in the computational grid. The half cylindrical grid structure was composed of three blocks: an upstream block, an effector section containing the micro-vanes, and a downstream block. See Figures (10) and (11). The computational half-plane grid varied in total number of mesh points from about 950,000 to 1,150,000 depending on the micro-vane configuration. All CFD calculations were

accomplished assuming half cylindrical symmetry. A two-equation k-l turbulence model was used in this study. The model consists of transport equation for the turbulent kinetic energy and turbulent length scale. The model includes a near-wall model and compressible corrections for high speed flows.

Harmonic Analysis of Distortion

The overall methodology used to obtain the harmonic content of inlet distortion was first proposed by Ludwig[12] and is currently in use at the Williams International Corporation. This methodology is characterized by the use of radial weighting factors applied to the total pressure rake measurements. The radial weighting factors are shown in Table (7).These radial weighting factors compress the rake information to a single radius ring of data samples, where the number of data samples corresponds to the number of arms of the measurement rake. A separate study was initiated by Anderson and Keller[13] to evaluate the impact of rake geometry (specifically the number of rake arms) on the measurement error associated with estimating the first five Fourier harmonic 1/2-amplitudes of engine face distortion. As a result of that study, the rake and methodology chosen for this study was the 80-probe "clocked" AIP rake because it provided the lowest error in estimating the first five Fourier harmonic 1/2-amplitudes of engine face distortion. Clocking the AIP rake means that N separate measurements were taken, and at each separate measurement, the angular orientation of the rake was advanced by an amount 1/N time the rake angle. The rake angle is the ratio of 360^{o} divided by the number of arms in the AIP rake. For example, a standard 80-probe rake has 16-arms. Hence the rake angle is 22.5^{o}. Therefore total pressure measurements were obtained at each 22.5^{o}/N angular position of the rake. Using the AIP instrumentation locations for the 80-probe rake, the 27 CFD solutions were interpolated at each of the probe positions shown in Figure (13a). The span-weighted average total pressure was calculated for the 80-probe rake by multiplying the probe total pressure by the span-weighted coefficients from Table (7), and adding the results over the five probes of the rakes to form a single radius ring of data samples.

Since the rake at the engine face was "clocked", a complete set of "repeats" was generated at each experimental run in Table (6). From the engine face patterns at each of the 10 clocking angles, a Fourier analysis was performed on the sample set of data and a standard deviation of the "repeats", S_{clock}, was determined for each of the Fourier harmonic 1/2-amplitudes. In order to check the constant variance assumption associated with least square regression, a simple F-test for comparing the minimum standard deviation to the maximum standard deviation ($F = S^2_{max}/S^2_{min}$) was conducted for each of the five responses. The results are presented in Table (8). Since each F-test exceeded the 95% confidence critical value of $F(0.975,9,9) = 4.03$, the assumption of constant variance across the design space had to be discarded. This meant that a regression technique known as weighted least squares regression had to be employed for analyzing the 10 x 27 = 270 data samples in the DOE. The weights in these regression analyses were set to $1/S^2_{clock}$.

The data reduction for the inlet total pressure recovery and engine face distortion differed greatly from the harmonic analysis of distortion described. There exists no recognized methodology to evaluate the Fourier harmonic 1/2-amplitudes of engine face distortion for more than five probes in the radial direction. Hence, evaluating the Fourier harmonic 1/2-amplitude directly from the computational mesh had to be discarded. However, both the inlet total pressure

recovery and engine face distortion can and were calculated directly from the computational grid at the engine face station. This computational mesh was composed of 49 x 121 grid points in the full-plane. The DC60 engine face distortion descriptor is defined such that it can be determined from either a computational grid or a standard measurement rake.[14] It is the only recognized distortion descriptor that has this property, and hence, was chosen for this study. The DC60 engine face distortion descriptor is a measure of the difference between the engine face or AIP average total pressure (PFAVE) and the lowest average total pressure in any sector defined by a critical angle of 60^{o} (PAVCRIT), divided by the average dynamic pressure at the engine (AIP) face. Hence,

$$DC60 = \frac{(PFAVE - PAVCRIT)}{QAVE} \qquad (3)$$

The CFD performance results for the Central Composite Face-Centered combined array DOE format involving both the factor (design) variables and the environmental (mission) variables are presented in Table (9). The inlet recovery (PFAVE) and the engine face distortion (DC60) were determined from the computation mesh. The Fourier harmonics 1/2-amplitudes of engine face distortion listed in Table (9) were determined from a "clocked" engine face rake and are the mean values over the 10 clocking angles. However, these values were not used in the regression analysis since weighted regression were required as a result of a lack of constant variance across the design space. Instead, the complete set of 10 x 27 = 270 values together with their corresponding weighting factors were used in the weighted regression to obtain the response surfaces for each of the Fourier harmonic 1/2-amplitudes of distortion.

Once the response surfaces are determined encompassing the inlet design parameters and mission variables, conceptual studies can be made to the determine the best and most cost effective method to manage the inlet flow field over the mission variable range. This type of conceptual study is not possible within a traditional Taguchi *Robust Parameter Design* methodology because the performance information of that installation over the outer array (mission) variable range is lost. These two sources of information are combined into a Taguchi signal-to-noise parameter (S/N) and are not contained in the regression.

Optimal Flow Control Over the Mission Variable Range

To illustrate the potential of RSM and *Robust Optimization Concepts* to design and optimize MSFC installations, three mission strategies were considered for the subject inlet, namely (1) Maximum Performance, (2) Maximum Engine Stability, and (3) Maximum HCF Life Expectancy. The Maximum Performance mission minimized the inlet total pressure losses, the Maximum Engine Stability mission minimized the engine face distortion, while the Maximum HCF Life Expectancy mission minimized the mean of the first five Fourier harmonic amplitudes, i.e. "collectively" reduced all the harmonic 1/2-amplitudes of engine face distortion. Each of the mission strategies was subject to a low engine face distortion constraint, i.e. $DC60 \leq 0.10$, which is a level acceptable for commercial engines, and a constraint on each individual Fourier harmonic 1/2-amplitudes: $Fk/2 \leq 0.015$, k = 1,2...5. For each of three mission strategies, i.e Maximum Performance, Maximum Engine Stability, and Maximum HCF Life Expectancy mission, an "Optimal Robust" (open loop control) and an "Optimal Adaptive" (closed loop control) installation were

designed to operate over an inlet throat Mach number range from 0.30 to 0.70, and angle-of-incidence range from 0.0^{o} to 20.0^{o}. The "Optimal Robust" installation arrived at a single MSFC installation which operated optimally over the entire throat Mach number and angle-of-incident range (open loop control). The "Optimal Adaptive" installation optimized all the design parameters at each throat Mach number and angle-of-incidence. Thus the "Optimal Adaptive" installation would require a closed loop control system to sense a proper signal for each effector and modify that effector device, whether mechanical or fluidic, for optimal inlet performance.The inlet throat Mach number and angle-of incidence range were the Taguchi noise or environmental variables over which each optimal installation had to be robust. A detailed description of the robust methodology used in the present study appears in Anderson and Keller,[4] and is termed the "Lower Order" method, while a lengthy comparison between the "Lower Order", Taguchi and an alternative "High Order" method appears in Anderson and Keller.[6]

Maximum Performance Mission - Two different inlet control strategies were considered for the Maximum Performance mission, an "Optimal Adaptive" and an "Optimal Robust" strategy. The "Optimal Adaptive" strategy optimized all the design parameters at each throat Mach number and angle-of-incidence, while "Optimal Robust" strategy arrived at a single MSFC installation which operated optimally over the entire throat Mach number and angle-of-incident range. To obtain the "Optimal Adaptive" Maximum Performance optimal installation designs, the inlet duct losses:

$$Y_{i,j} = (1 - PFAVE)_{i,j} \qquad (4)$$

where minimized at each of the N_M values of inlet throat Mach numbers and each of the N_α angles-of-incidence to obtained the optimal installation corresponding to that inlet operating condition. This search was subject to the engine face distortion constraint that

$$DC60 \leq 0.10 \qquad (5)$$

while the individual Fourier harmonic 1/2-amplitudes of distortion were each constrained to

$$\frac{Fk}{2} \leq 0.015 \qquad (6)$$

where k = 1 to 5. In a similar manner, the "Optimal Robust" Maximum Performance installation design was determined through a search process to locate that installation geometry that minimized the decision parameter:

$$Y_{M,\alpha} = \frac{1}{N_M} \sum_{i=1}^{N_M} \frac{1}{N_\alpha} \sum_{j=1}^{N_\alpha} (1 - PFAVE)_{i,j} \qquad (7)$$

where N_M is the number of throat Mach number conditions in the set from Mt = 0.30 to 0.70, and N_α is the number angles-of-incidence α = 0.0 to 20.0°. This search was also subject to the engine face distortion constraint that

$$DC60 \leq 0.10 \quad (8)$$

and the individual Fourier harmonic 1/2-amplitudes of distortion constraint to

$$\frac{Fk}{2} \leq 0.015 \quad (9)$$

Comparisons between the performance results of the "Optimal Robust" and "Optimal Adaptive" installations for the Maximum Performance inlet mission are shown in Figure (14). Also presented in Figures (14) is the inlet baseline performance at an inlet throat Mach number of 0.70 for each response. It is apparent from Figure (14) that flow control was able to increase total pressure recovery substantially above the baseline flow at 0.70 inlet throat Mach number. This was not the case for the high strength micro-vane effector units.[4]-[5]

The "Optimal Robust" and "Optimal Adaptive" installations provided essentially the same performance over the inlet throat Mach number range for 0.30 to 0.70 and angle-of-incidence range of 0° to 20°. This is not surprising, since there exists experimental data[11] that demonstrate that a fixed secondary flow control installation optimally designed can provide essentially the same low DC60 distortion level, i.e. $DC60 \leq 0.10$, over a substantial angle-of-incidence range. Secondary flow control in inlets is inherently robust, provided it is optimally designed. In addition, "Optimal Robust" and "Optimal Adaptive" installations reduced all the Fourier harmonic 1/2-amplitudes to a value of 0.01 or below, which is extremely low. Although a correlation between engine face distortion and the Fourier harmonic 1/2-amplitudes can not be established, reducing the Fourier harmonic 1/2-amplitudes is essentially the same at reducing the engine face circumferential distortion.

In order to validate the DOE prediction results, a set of nine cases was run using the "Optimal Robust" installation design determined from the search procedure described. The validation cases are defined in Table (10) and were organized as a full factorial array with the two mission variables at three levels each, i.e. 3^2 cases. Each of the 9 CFD cases in Table (10) were run with a Reynolds-averaged Navier-Stokes code, and the performance results are presented in Table (11). More will be said about these performance results later in the report. However, the performance of the "Optimal Robust" installation design were excellent. The engine face total pressure recovery contours for 9 CFD validation cases defined in Table (10) are presented in Figure (15). The circumferential uniform nature of the engine face distortion patterns over the range of inlet throat Mach numbers from 0.30 to 0.70 and inlet angles-of-incidences from 0.0° to 20.0° can clearly be seen in Figure (15).

The near wall streamlines for the baseline solution and the "Optimal Robust" Maximum Performance installation design are presented in Figures (16a) and (16b) respectively for an inlet throat Mach number of 0.30 and inlet angle-of-incidence α = 0.0°. A comparison of these two figures indicates the underlying operational purpose of micro-scale secondary flow

effector devices. In the baseline flow presented in Figure (16a), secondary motion or "over-turning" of the fluid, arises through an inbalance between centrifugal force and radial pressure gradient at wall of the first bend in the S-duct. This inbalance displaces high-speed fluid towards the outer (concave) wall and low-speed fluid towards the inner (convex) wall and leads to a generation of longitudinal vorticity which tend to congregate on the inner (convex) wall of the first bend. This forms the vortex pair in the inlet S-duct, which eventually "lifts-off". See Figure (2). This vortex pair results in total pressure loss and severe total pressure distortion at the engine face. It is not necessary for this vortex to "lift-off" or separate from the walls for high total pressure loss and distortion to occur (hence the terminology inlet "secondary flow control" rather than "separation control"). By introducing the micro-vane effectors into the inlet the "over-turning" in the inlet boundary is prevented. See Figure (15b). Consequently, the passage vortex will not form or, at worst, is greatly reduced in strength, which will results in a vast improvement in engine face distortion. Therefore, the entire inlet flow field can be managed by controlling the secondary flow in a thin layer adjacent to the inlet walls.

Maximum Engine Stability Mission - To obtain the "Optimal Adaptive" Maximum Engine Stability installation designs, a search was made over the factor variable space to locate that installation geometry that minimized the decision parameter:

$$Y_{i,j} = (DC60)_{i,j} \qquad (10)$$

at each throat of the N_M inlet throat Mach numbers and each of the N_α inlet angles-of-incidence. This search was subject to the constraint that each Fourier harmonic 1/2-amplitude of distortion satisfy the relationship:

$$\frac{Fk}{2} \leq 0.015 \qquad (11)$$

where k = 1 to 5, while no constraint was placed on the inlet total pressure recovery (PFAVE). In a similar manner, the "Optimal Robust" Maximum Engine Stability installation design was determined through a search process to locate that installation geometry that minimized the decision parameter:

$$Y_{M,\alpha} = \frac{1}{N_M}\sum_{j=1}^{N_M}\frac{1}{N_\alpha}\sum_{i=1}^{N_\alpha}(DC60)_{i,j} \qquad (12)$$

where N_M is the number of throat Mach number conditions in the set from Mt = 0.30 to 0.70, and N_α is the number of angles-of-incidence α = 0.0 to 20.0°. This search was also subject to the constraint that

$$\frac{Fk}{2} \leq 0.015 \qquad (13)$$

while no constraint was placed on the inlet total pressure recovery (PFAVE).

Comparisons between the performance results of the "Optimal Robust" and "Optimal Adaptive" installations for the Maximum Engine Stability inlet mission are shown in Figure (17). Also presented in Figure (17) is the inlet baseline performance at an inlet throat Mach number of 0.70 for each response. It is apparent from Figure (17) that both the "Optimal Robust" and "Optimal Adaptive" installations were able to increase total pressure recovery substantially well above the baseline flow at 0.70 inlet throat Mach number with an unconstrained inlet total pressure recovery (PFAVE) condition during the search procedure. While no correlation can be established between engine face distortion and inlet total pressure recovery, this occurrence suggest that maximum inlet total pressure recovery occurs when the engine face circumferential distortion approaches zero.

In order to validate the DOE prediction for the "Optimal Robust" Maximum Engine Stability installation performance results, a set of nine cases were run using the "Optimal Robust" installation design determined from the search procedure described. The validation cases are defined in Table (12) and were also organized as a full factorial array with two mission variables at three levels, i.e. 3^2 cases. Each of the 9 CFD cases in Table (12) were run with a Reynolds-averaged Navier-Stokes code, and the performance results are presented in Table (13). More will be said about these performance results later in the report. However, the performance of the "Optimal Robust" Maximum Engine Stability installation design were excellent. The engine face total pressure recovery contours for the 9 CFD validation cases defined in Tables (12) are presented in Figure (18). Again, the circumferential uniform nature of the engine face distortion patterns over the range of inlet throat Mach numbers from 0.30 to 0.70 and inlet angles-of-incidence from 0.0^{o} to 20.0^{o} can clearly be seen in Figure (18).

Presented in Figure (19) are the near wall streamlines for the baseline inlet solution and "Optimal Robust" Maximum Engine Stability installation design at a throat Mach number of 0.50 and inlet angle-of-incidence, $\alpha = 10.0^{o}$. Again, notice the effect of the micro-vane actuators in preventing the over-turning of the flow adjacent to the inlet walls and thus suppressing the passage vortex formation.

Maximum HCF Life Expectancy Mission -The "Optimal Adaptive" Maximum HCF Life Expectancy MSFC installation was determined through a search process over the factor variable space to locate that installation geometry that minimized the mean of the first five Fourier harmonic 1/2-amplitudes of distortion, i.e

$$Y_{i,j} = \frac{1}{5}\sum_{k=1}^{5}\left(\frac{Fk}{2}\right)_{i,j} \qquad (14)$$

at each of the N_M inlet throat Mach numbers and each of the N_α inlet angles-of-incidence. This defined the "Optimal Adaptive" installation design at each of these inlet operating conditions subject to inlet total pressure recovery (PFAVE) being unconstrained and the following constraint on the engine face distortion:

$$DC60 \le 0.01 \qquad (15)$$

and constraint on the individual Fourier harmonic 1/2-amplitudes of distortion
:

$$\frac{Fk}{2} \leq 0.015 \qquad (16)$$

where k = 1 to 5. The "Optimal Robust" Maximum HCF Life Expectancy MSFC installation was also determined through a search process over the factor variable space to locate that installation geometry that minimized the decision parameter:

$$Y_{M,\alpha} = \frac{1}{N_M}\sum_{i=1}^{N_M}\frac{1}{N_\alpha}\sum_{j=1}^{N_\alpha}\frac{1}{5}\sum_{k=1}^{5}\left(\frac{Fk}{2}\right)_{i,j} \qquad (17)$$

where N_M is the number of throat Mach number conditions in the set from Mt = 0.30 to 0.70, and N_α is the number angles-of-incidence α = 0.0 to 20.0°. This search was also subject to and unconstrained inlet total pressure recovery (PFAVE) and the constraint that the engine face distortion satisfy the relationship:

$$DC60 \leq 0.10 \qquad (18)$$

and each Fourier harmonic 1/2-amplitude satisfy the expression:

$$\frac{Fk}{2} \leq 0.015 \qquad (19)$$

Comparisons between the performance results of the "Optimal Robust" and "Optimal Adaptive" installations for the Maximum HCF Life Expectancy mission are shown in Figure (20). Also presented in Figure (20) is the inlet baseline performance at an inlet throat Mach number of 0.70 for each response. It is apparent from Figure (20) that both the "Optimal Robust" and "Optimal Adaptive" installations were able to increase total pressure recovery substantially above the baseline flow at 0.70 inlet throat Mach number with an unconstrained inlet total pressure recovery (PFAVE) condition during the search procedure. While no correlation can be established between the Fourier harmonic 1/2-amplitudes and engine face distortion or inlet total pressure recovery, this occurrence suggest that maximum inlet total pressure recovery occurs when the Fourier harmonic 1/2-amplitudes of distortion approach zero.

In order to validate the DOE prediction for the "Optimal Robust" Maximum HCF Life Expectancy installation performance results, a set of nine cases were run using the "Optimal Robust" installation design determined from the search procedure described. The validation cases are defined in Table (14) and were organized as a full factorial array with the two mission variables at three levels, i.e. 3^2 cases. Each of the 9 CFD cases in Table (14) were run with a Reynolds-averaged Navier-Stokes code, and the performance results are presented in Table (15). The engine face total pressure recovery contours for the 9 CFD validation cases defined in Table (14) are presented in Figure (21). Again, the circumferential uniform nature of the engine face distor-

tion patterns over the range of inlet throat Mach numbers from 0.30 to 0.70 and inlet angles-of-incidences from 0.0^{o} to 20.0^{o} can clearly be seen in Figure (21).

The near wall streamlines for the baseline inlet solution and "Optimal Robust" Maximum HCF Life Expectancy installation design at a throat Mach number of 0.70 and inlet angle-of-incidence of $\alpha = 20.0^{o}$ are presented in Figure (22a) and (22b) respectively. Again, notice the effect of the micro-vane actuators in preventing the over-turning of the flow adjacent to the inlet walls. This suppresses the formation of the passage vortex, thus resulting in the engine face distortion patterns displayed in Figure (21).

Comparison of the Optimal Robust Installation Designs

Comparison of the performance of the three "Optimal Robust" installation designs, i.e. the Maximum Performance, Maximum Engine Stability, and Maximum HCF Life Expectancy mission designs, are shown in Figures (23) through (25) at a throat Mach number of 0.70 and an inlet angle-of-incidence of 20.0^{o}. These figures also include the baseline inlet performance, i.e. the performance of the redsigned M2129 inlet S-duct without flow control. The low strength effector units used in these designs achieved a substantial improvement in inlet total pressure recovery (PFAVE) over the baseline performance. See Figure (23). This differs from the performance of the high strength effector units which never increased the inlet total pressure recovery above the baseline value[4]. Excellent engine face distortion characteristics were also achieved with the low strength effector units as shown in Figure (24). Although very low engine face distortion was also achieved with the high strength effector units[4], the overall installation reductions were substantially greater than the present designs. Presented in Figure (25) is a comparison of the first five Fourier harmonic 1/2-amplitudes for the three "Optimal Robust" installation designs with the baseline inlet characteristics. Minimizing the mean of the first five Fourier harmonic 1/2-amplitudes resulted in a substantial reduction in the amplitudes of the first three harmonics 1/2-amplitudes, and very low amplitudes for the fourth and fifth harmonic components.

By visually comparing the performance of the three "Optimal Robust" installations designs presented in Figures (23) through (25), it is obvious that they are remarkably similar. This similarity can be established objectively by a statistical comparison between the optimal CFD performance validations presented in Tables (11), (13) and (15). Since each of the nine CFD validation cases listed in these tables was run at the same conditions of throat Mach number and inlet angle-of-incidence, they represent a blocked set of results.

A comparison can be made between the mean or average values of two response variables, $\bar{Y}_i$ from the i-th data set and $\bar{Y}_j$ for the j-th data set using the t-statistic

$$t^* = \frac{\left|\bar{Y}_i - \bar{Y}_j\right|}{S_p\left(\frac{1}{N_i} + \frac{1}{N_j}\right)^{\frac{1}{2}}} \qquad (20)$$

Here the pooled standard deviation for the two sets of data is calculated from the equation:

$$S_p = \sqrt{\frac{(N_i - 1)S_i^2 + (N_j - 1)S_j^2)}{(N_i - 1) + (N_j - 1)}} \quad (21)$$

assuming S_i^2 and S_j^2 are not significantly different base on the F-test. The two standard deviations used in equation (21) are calculated as follows:

$$S_i = \sqrt{\frac{\sum_{k=1}^{N_i} (Y_{i,k} - \overline{Y}_i)^2}{N_i - 1}} \quad (22)$$

and

$$S_j = \sqrt{\frac{\sum_{k=1}^{N_i} (Y_{j,k} - \overline{Y}_j)^2}{N_i - 1}} \quad (23)$$

The F-test is based on the ratio S_i^2 and S_j^2.

Comparison between the standard deviation from data set (i) with the standard deviation from data set (j) can be made through the expression:

$$F^* = \frac{S_{larger}^2}{S_{smaller}^2} \quad (24)$$

where S_{larger} is the larger standard deviation from either data set (i) or (j), and $S_{smaller}$ is the smaller standard deviation from either data set (i) or (j). The standard deviation S_i from the i-th data set is not statistically different from the standard deviation S_j from the j-th data set at the 95% confidence level if the relationship

$$F^* < F(0.975, \nu_i, \nu_j) \quad (25)$$

holds. Likewise, the standard deviation S_i from the i-th data set is statistically different from the standard deviation S_j from the j-th data set at the 95% confidence level if the relationship

$$F^* > F(0.975, \nu_i, \nu_j) \quad (26)$$

is true. In equations (25) and (26), $F(0.975, \nu_i, \nu_j)$ is the 95% percentile of the standard F-distribution F-value with ν_i degrees of freedom in the numerator and ν_j degrees of freedom in the dominator. The degrees of freedom from the i-th data set is given by:

$$\nu_i = (N_i - 1) \quad (27)$$

while the degrees of freedom from the j-th data set is given by:

$$\nu_j = (N_j - 1) \quad (28)$$

When the difference between the minimum value of the response variable and the maximum value of the response variable in a DOE is a decade or greater, there often exist a linear relationship between the mean response and the standard deviation. Under this condition, the logarithm of the response will stabilize the variation over the range of the response. Because this was the case with DC60 and the Fourier harmonic 1/2-amplitudes over the DOE variable space, the natural logarithm of the response variable was used in the DOE analysis and in this analysis of means. However, the inlet total pressure recovery (PFAVE) was not transformed in the DOE analysis and hence was not transformed in this evaluation of means.

Therefore, a direct statistical comparison can be made between the mean values of the response $\ln(Y_i)$ and $\ln(Y_j)$ of two data set (i) and (j) which have been transformed using a natural logarithmic function by the t-statistic:

$$t^* = \frac{\left|\overline{\ln(Y_i)} - \overline{\ln(Y_j)}\right|}{S_p\left(\frac{1}{N_i} + \frac{1}{N_j}\right)^{\frac{1}{2}}} \quad (29)$$

where N_i is the number of values in data set (i), N_j the number of values data set (j), and S_p is the "pooled" standard deviation defined by the relationship:

$$S_p = \sqrt{\frac{(N_i - 1)S_i^2 + (N_j - 1)S_j^2)}{(N_i - 1) + (N_j - 1)}} \quad (30)$$

and mean of the transformed response variable for the i-th data set is given by:

$$\overline{\ln(Y_i)} = \frac{1}{N_i}\sum_{k=1}^{N_i} \ln(Y_{i,k}) \quad (31)$$

while the mean of the transformed response variable for the j-th data set is determined from the expression:

$$\overline{\ln(Y_j)} = \frac{1}{N_j}\sum_{k=1}^{N_j} \ln(Y_{j,k}) \qquad (32)$$

The standard deviation from the i-th data set can be determined from the equation:

$$S_i = \sqrt{\frac{\sum_{k=1}^{N_i} (\ln(Y_{i,k}) - \overline{\ln(Y_i)})^2}{N_i - 1}} \qquad (33)$$

while the standard deviation from the j-th data set can be computed from the equation:

$$S_j = \sqrt{\frac{\sum_{k=1}^{N_j} (\ln(Y_{j,k}) - \overline{\ln(Y_j)})^2}{N_j - 1}} \qquad (34)$$

where $\overline{\ln(Y_i)}$ and $\overline{\ln(Y_j)}$ are obtained from equations (31) and (32).

In comparing the mean values from two data sets (i) and (j), if the expression

$$t^* < t(0.975, \nu_p) \qquad (35)$$

is valid, the response values from the i-th data set are not statistically different from the response values from the j-th data at the 95% confidence level. Likewise, the response values from the i-th data set are statistically different from the response values from the j-th data set at the 95% confidence level if the expression

$$t^* > t(0.975, \nu_p) \qquad (36)$$

holds. The term ν_p is the "pooled" degrees of freedom given by the expression:

$$\nu_p = (N_i - 1) + (N_j - 1) \qquad (37)$$

and $t(0.975, \nu_p)$ is the is the 95% confidence t-value for ν_p degrees of freedom.

The results of the t-tests for the comparison of the means and F-tests for comparison of the standard deviations based on the CFD validation cases presented in Tables (11), (13) and (15) are shown in Tables (16) through (21). The evaluations presented in Tables (16) through (21) have been organized as three sets of comparisons for mean and standard deviations of two "Optimal Robust" mission installation designs. In the first comparison, the mean and standard deviations between the Maximum Performance (data set 1) and Maximum Engine Stability (data

set 2) mission cases are evaluated for eight response variables. This comparison is presented in Tables (16) and (17). In the second comparison set, the mean and standard deviations between the Maximum Performance (data set 1) and Maximum HCF Life Expectancy (data set 3) mission cases are evaluated, again for the same eight response variables. This comparison is presented in Tables (18) and (19). Tables (20) and (21) present the results for the third set of comparisons, i.e. between the mean and standard deviations of the Maximum Engine Stability (data set 2) and Maximum HCF Life Expectancy (data set 3) mission cases for the same eight response variables. The eight response variables evaluated were the inlet total pressure recover (PFAVE), the engine face distortion (DC60), the first five Fourier harmonic 1/2-amplitudes of distortion (F1/2,F2/2, F3/2,F4/2,F5/2), and the mean of the first five Fourier harmonic 1/2-amplitudes of distortion (FM/2). The results of this study indicated that there were no statistical significant differences between the three sets of CFD validations cases presented in Tables (11), (13), and (15) at the 95% confidence level. Even though there are differences in the factor variables that define the "Optimal Robust" installation designs, these factor differences did not translate into statistically significant inlet performance differences over the range of throat Mach Numbers from 0.30 to 0.70 and inlet angle-of-incidences from 0^{o} to 20.0^{o}.

Although the three "Optimal Robust" installation designs were generated from three very different mission strategies, the performance achieved by these installation designs were not statistically significantly different over the entire mission variable range. Hence one can draw overall conclusions with regard to the micro-scale secondary flow control installation design. Since the common dominator in each of the "Optimal Robust" installation designs was that the engine face circumferential distortion in each case were all driven to near zero, one can conclude that this condition represents the most robust operating state of the inlet. In other words, the inlet is most tolerant to mission variable disturbances when there is no circumferential distortion. Although there is no established correlation between circumferential distortion and any of the Fourier harmonics 1/2-amplitudes, minimizing the mean of the first five Fourier harmonic 1/2-amplitudes of distortion results in driving the circumferential distortion to near zero. Likewise, one can also conclude that the inlet achieves its highest total pressure recovery when the circumferential distortion is also driven to zero, even though there is no established correlation between total pressure recovery and circumferential distortion. The near zero engine face circumferential distortion was provided by the three "Optimal Robust" micro-scale secondary flow installation designs over the entire mission variable range. The "Optimal Robust" installation designs also provide essentially the same performance as the "Optimal Adaptive" over the same mission variable range.

Statistical Comparison of CFD Analysis and DOE Predictions

Extensive CFD validation cases were included in this study and these are presented in Tables (11), (13) and (15). There are a total of 27 CFD validation cases. They represent the three "Optimal Robust" installation designs determined by the "Lower Order" Robust design methodology[4]. The CFD validation performance results for "Optimal Robust" Maximum Performance, Maximum Engine Stability installation, and Maximum HCF Installation designs included all the response variables important for this study, i.e. inlet total pressure recovery (PFAVE), engine face distortion (DC60), and the first five Fourier harmonic 1/2-amplitudes of distortion (F1/2, F2/2, F3/2, F4/2, and F5/2). These results indicate that the three "Optimal Robust" installa-

tion designs satisfied the design requirements over the entire mission variable range. In order to validate the DOE performance prediction procedure, three cases from each of the set of CFD performance validation cases were chosen for statistical comparison with the DOE predictions.

A direct statistical comparison can be made between the optimal responses predicted by the DOE models (Y_{DOE}) and the actual CFD predicted performance values (Y_{CFD}) through the expression:

$$t^* = \frac{\left|\ln(Y_{CFD}) - \ln(Y_{DOE})\right|}{\frac{\ln(Y_A) - \ln(Y_{DOE})}{t(0.975, N-p)}} \qquad (38)$$

where Y_A is the upper 95% confidence interval for the individual predicted response Y_{DOE} from the regression model, and t(0.975,N-p) is the 95% confidence t-value for N-p degrees of freedom. As previously discussed, when there exist a functional relationship between the mean values and standard deviation of the data, the data set does not satisfy the requirement of a normally distributed set. Under this condition, a transformation is often used to stabilize the variation over the response variable range. Because this was the case with DC60 and the Fourier harmonic 1/2-amplitudes, the natural logarithm of these responses were used in the DOE analysis, the analysis of means and variances described in the previous section, and in this evaluation of the DOE model. Since all the response parameters except for PFAVE were analyzed using a natural log transformation, the natural log of the response (Y) was used in the statistical comparison of those response variables. For a statistically significant difference to exist between the DOE model predicted response (Y_{DOE}) and the CFD validation response prediction (Y_{CFD}), the expression:

$$t^* > t(0.975, N-p) \qquad (39)$$

must hold. Likewise, if the expression

$$t^* < t(0.975, N-p) \qquad (40)$$

is valid, the Y_{CFD} is not statistically different from Y_{DOE}. Therefore, for no significant statistical difference to exist between the DOE model predicted response Y_{DOE} and the CFD analysis response Y_{CFD}, the CFD response prediction must fall within the 95% confidence interval of the DOE model prediction for that response. For each "Optimal Robust" installation design, the statistical comparisons were made using the diagonal three cases in each set listed in Tables (11), (13) and (15).

Tables (19) through (21) show the results of this statistical comparison over the range of throat Mach Numbers from 0.30 to 0.70 and inlet angle-of-incidences from 0^o to 20.0^o for the Maximum Performance, Maximum Engine Stability, and Maximum HCF Life Expectancy missions. In general, the number of incidences when the comparisons were statistically different was somewhat above 5%, which is remarkably good. All the cases in which a statistical difference were indicated involved in the evaluation of the Fourier harmonic 1/2-amplitudes of distortion. In these particular cases, the differences between the CFD analysis and DOE prediction were to too

small to be of practical significance This indicates that the DOE prediction results are not substantially different from the CFD analysis results (i.e. the CFD analysis predictions fell within the 95% confidence interval of the DOE performance predictions). It also indicates that the optimal installations determined by the DOE models were a statistically valid optima when compared to the actual CFD installation analyses. The accuracy of the response surfaces determined from the DOE analysis was therefore more than adequate for use in determining an installation optimum and for conceptual studies on the inlet-engine control system design.

CONCLUSIONS

The fundamental importance of Genichi Taguchi's contribution to RSM over traditional design approaches lies in the idea that process and product sensitivity to their environment can be incorporated into the optimal statistical Design-of-Experiment and subsequent analysis of the data. The Taguchi noise factors that cause variability in industrial design are often the environmental variables, such as temperature and humidity, properties of the material, and product aging. In aerodynamic design, the Taguchi noise factors can be identified with the mission variables, since they produce variation from the design condition. Being able to include the mission variables directly into the inlet design process represents a major breakthrough in the area of aerodynamic design of inlets. The inlet system can now be designed to operate with optimal performance over a range of specified mission variables.Taguchi's *Robust Parameter Design* method, however, may not be optimal in the design of secondary flow installations for inlet systems because: (a) it loses information vital to the aerodynamicist and, (b) it is costly. Fortunately, the important aspects surrounding Taguchi's approach to *Robust Parameter Design* can and have been incorporated into an alternate economical approach and adapted to the inlet design problem. This alternate inlet design method, using a combined array approach to economical Robust Design, had a significant run size savings over a traditional Taguchi approach, i.e. 27 CFD experiments as compared to 45 CFD experiments. The combined array DOE format, in which the factor (design) variables are included with the environmental (mission) variables, allows for conceptual studies to me made on the inlet-engine control system to determine the most efficient and cost effective system prior to any experimentation. These conceptual studies on the inlet-engine control system can not be made using Taguchi's *Robust Parameter Design* methodology.

To illustrate the potential of economical Robust Design methodology, three different mission strategies were considered for the subject inlet, namely (1) Maximum Performance, (2) Maximum Engine Stability, and (3) Maximum HCF Life Expectancy. The Maximum Performance mission minimized the inlet total pressure losses, the Maximum Engine Stability mission minimized the engine face distortion (DC60), while the Maximum HCF Life Expectancy mission minimized the mean of the first five Fourier harmonic amplitudes, i.e. "collectively" reduced all the harmonic 1/2-amplitudes of engine face distortion. Each of the mission strategies was subject to a low engine face distortion constraint, i.e. $DC60 \leq 0.10$, which is a level acceptable for commercial engines, and a constraint on each individual Fourier harmonic amplitudes of $Fk/2 \leq 0.015$. For each of these missions strategies, an "Optimal Robust" (open loop control) and an "Optimal Adaptive" (closed loop control) installation were designed over an inlet throat Mach number range from 0.30 to 0.70, and angle-of-incidence range from 0.0^{o} to 20.0^{o}. The "Optimal Robust" installation used economical Robust Design methodology to arrive at a single design which operated over the entire angle-of-incident range (open loop control). The "Optimal Adaptive" installation optimized all the

design parameters at each throat Mach number and angle-of-incidence. Thus the "Optimal Adaptive" installation would require a closed loop control system to sense a proper signal for each effector and modify that effector device, whether mechanical or fluidic, for optimal inlet performance. In general, the performance differences between the "Optimal Adaptive" and "Optimal Robust" installation designs were found to be marginal. This suggests, that "Optimal Robust" open loop installation designs can be very competitive with "Optimal Adaptive" close loop designs.

Effective inlet flow control management of engine face distortion was achieved by reducing the unit strength of the micro-vane effector and allowing the installation design to influence the inlet flow over an extended streamwise distance by substantially increasing the micro-vane chord length. With this combination, the total pressure losses associated with micro-vane effectors became very small, and a large overall performance gain achieved. In addition, this study demonstrated that optimal "low unit strength" micro-effector installation designs exhibited the same robustness properties as optimal "high unit strength" micro-effector installation, but without the large total pressure loss. The design strategy of replacing "high unit strength" micro-effectors with "low unit strength" micro-effectors which influence the flow over an extended streamwise distance was therefore found to be very effective.

REFERENCES

(1) Anderson, B. H., Miller, D. M., Yagel, P. J, and Traux, P. P., "A Study of MEMS Flow Control for the Management of Engine Face Distortion in Compact Inlet Systems", FEDSM99-6920, 3rd ASME/JSME Joint Fluids Engineering Conference, San Francisco, CA, July 18-23, 1999.

(2) Hamstra, J. W., Miller, D. N., Truax, P. P., Anderson, B. H., and Wendt, B. J., "Active Inlet Flow Control Technology Demonstration", ICAS-2000-6.11.2, 22nd International Congress of the Aeronautical Sciences, Harrogate, UK, August 27th-September 1st, 2000.

(3) Taguchi, G and Wu, Y, "Introduction to Off-Line Quality Control," Central Quality Control Association, 1980.

(4) Anderson, B. H. and Keller, D. J., "A Robust Design Methodology for Optimal Micro-Scale secondary Flow Control in Compact Inlet Diffusers", AIAA Paper No. 2002-0541, Jan. 2002.

(5) Anderson, B. H. and Keller, D. J., "Optimal Micro-Scale Secondary Flow Control for the Management of HCF and Distortion in Compact Inlet Diffusers", Proposed NASA TM, 2001.

(6) Anderson, B. H. and Keller, D. J., "Robust Design Methodologies for Optimal Micro-Scale Secondary Flow Control in Compact Inlet Diffusers", NASA/TM-2001-211477, March 2001.

(7) AGARD FTP Working Group 13, "Air Intakes for High Speed Vehicles", AR-270, September 1991.

(8) Willmer, A. C., Brown, T. W. and Goldsmith, E. L., "Effects of Intake Geometry on Circular Pitot Intake Performance at Zero and Low Forward Speeds", Aerodynamics of Power Plant Installation, AGARD CP301, Paper 5, Toulouse, France, May 1981, pp 51-56.

(9) Goldsmith, E. L. and Seddon, J. (eds), "Practical Intake Aerodynamics," Blackwell Scientific Publications, Oxford, 1993.

(10) Bender, E. E, Anderson, B. H., and Yagle, P. J., "Vortex Generator Modeling for Navier Stokes Code", FEDSM99-69219, 3rd ASME/JSME Joint Fluids Engineering Conference, San Francisco, CA, July 18-23, 1999.

(11) Gibb, J. and Anderson, B. H., "Vortex Flow Control Applied to Aircraft Intake Ducts," Proceedings of the Royal Aeronautical Society Conf., High Lift and Separation Control, Paper No. 14, Bath, UK, March, 1995.

(12) Ludwig, G. R., "Aeroelastic Considerations in the Measurement of Inlet Distortion", 3rd National Turbine Engine High Cycle Fatigue Conference, 1998.

[13] Anderson, B. H. and Keller, D. J., "Considerations in the Measurements of Engine Face Distortion for High Cycle Fatigue in Compact Inlet Diffusers", NASA/M-2001-211476, March 2001.

[14] Goldsmith, E. L., and Seddon, J. (eds), "Practical Intake Aerodynamics," Blackwell Scientific Publications, Oxford, 1993.

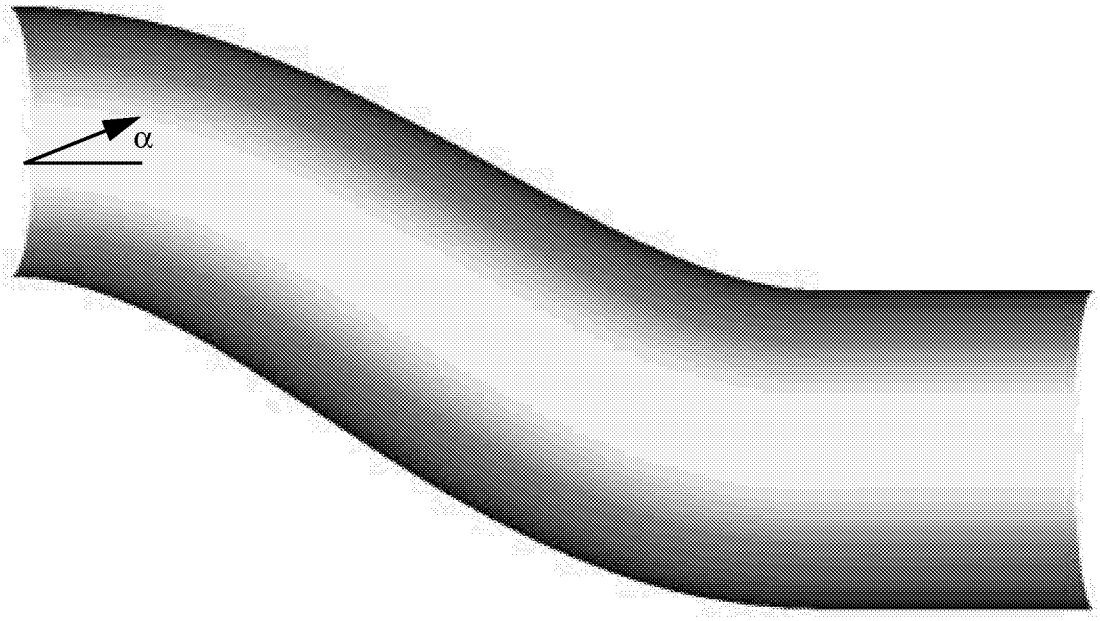

(a) Baseline Inlet S-Duct Geometry

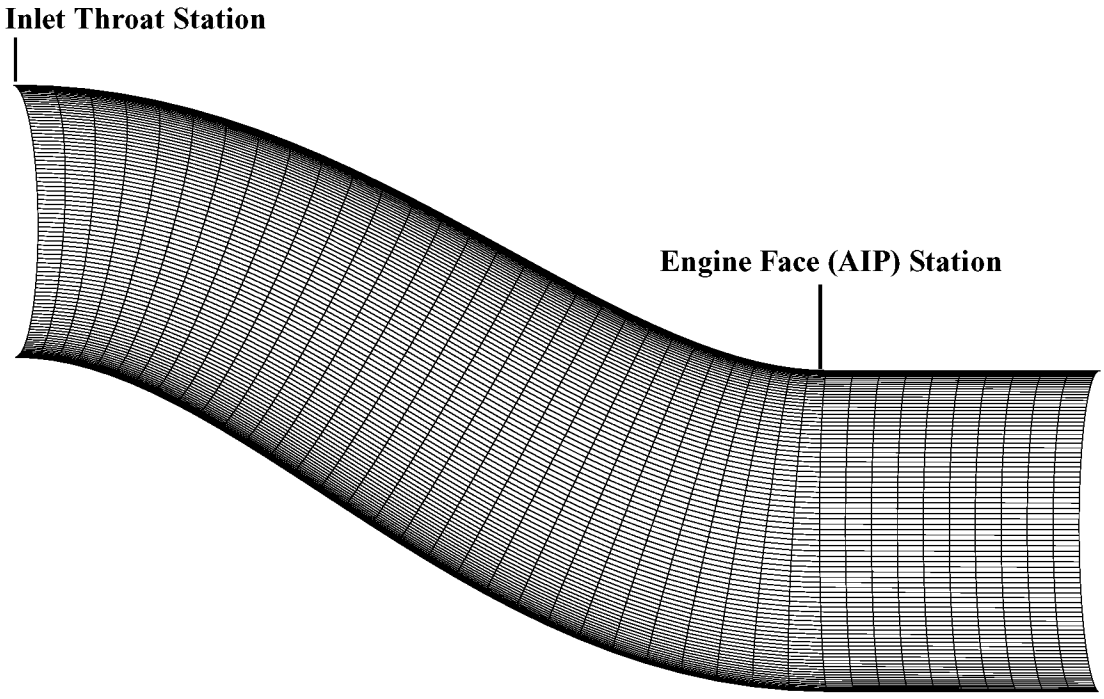

(b) Baseline Inlet S-Duct Computational Grid

Figure (1): Geometry and computational grid for redesigned M2129 inlet S-duct.

Config.	Mt	α (degs)
nvg301	0.30	0.0
nvg302	0.70	0.0
nvg303	0.30	20.0
nvg304	0.70	20.0
nvg305	0.30	10.0
nvg306	0.70	10.0
nvg307	0.50	0.0
nvg308	0.50	20.0
nvg309	0.50	10.0

Table (1): CFD validation cases for the baseline inlet S-duct.

Config.	PFAVE	DC(60)	F1/2	F2/2	F3/2	F4/2	F5/2
nvg301	0.99366	0.34109	0.00569	0.00577	0.00451	0.00294	0.00139
nvg302	0.96723	0.45485	0.03589	0.02951	0.01708	0.00498	0.00350
nvg303	0.98949	0.38795	0.00854	0.00747	0.00486	0.00227	0.00049
nvg304	0.95275	0.49219	0.04828	0.03409	0.01384	0.00154	0.00679
nvg305	0.99261	0.35889	0.00710	0.00677	0.00492	0.00270	0.00077
nvg306	0.96439	0.46496	0.03799	0.03052	0.01661	0.00399	0.00430
nvg307	0.98617	0.36363	0.01456	0.01363	0.01015	0.00553	0.00158
nvg308	0.97888	0.42716	0.01968	0.01668	0.01007	0.00379	0.00119
nvg309	0.98400	0.39474	0.01636	0.01490	0.01035	0.00498	0.00105

Table (2): Engine face performance results for the baseline inlet S-duct.

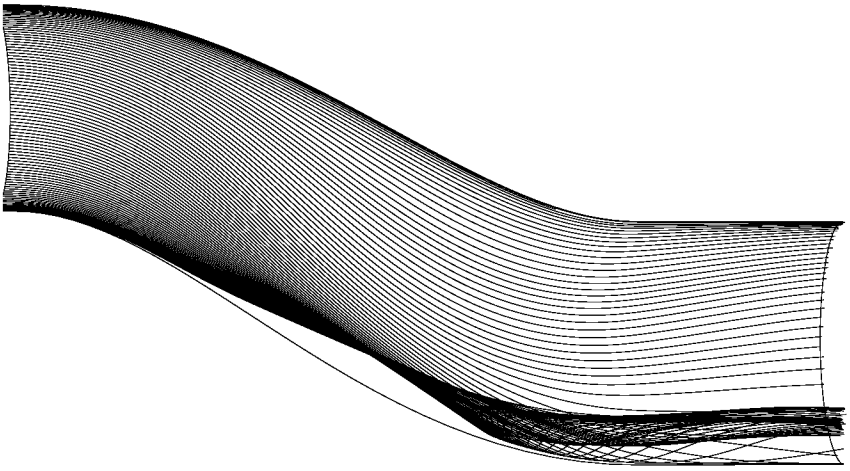

(a) Baseline Condition, Mt = 0.30, $\alpha = 0.0^{o}$

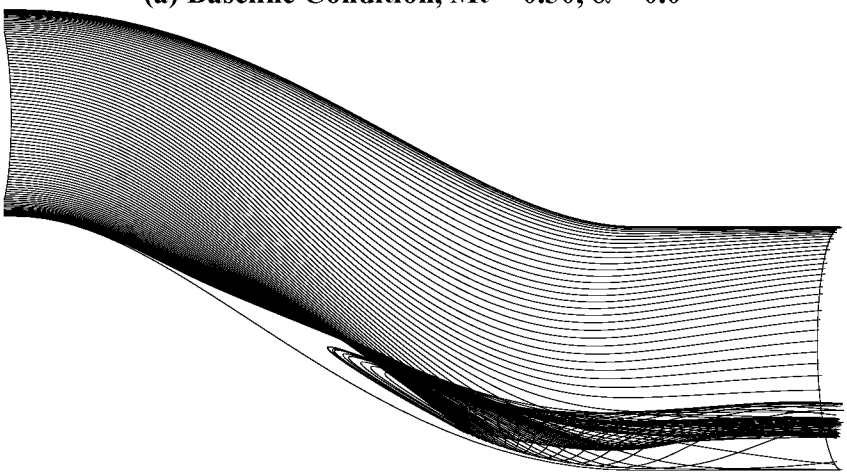

(b) Baseline Condition, Mt = 0.50, $\alpha = 10.0^{o}$

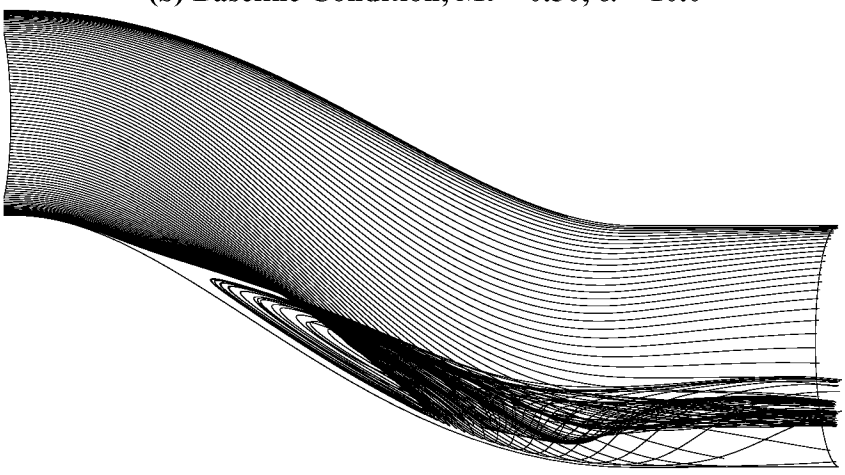

(c) Baseline Condition, Mt = 0.70, $\alpha = 20.0^{o}$

Figure (2): Near wall streamline traces in the baseline inlet S-duct.

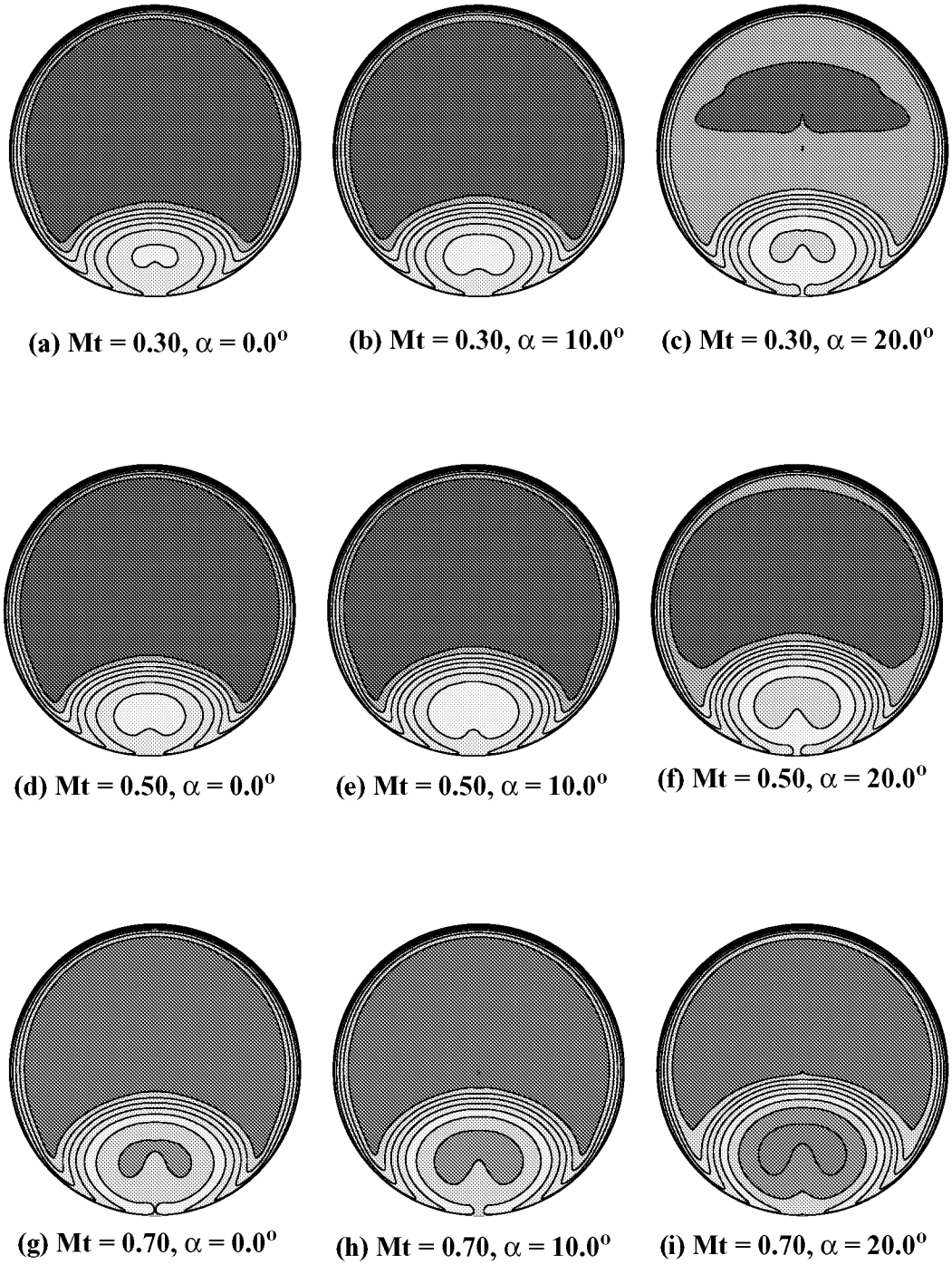

(a) Mt = 0.30, $\alpha = 0.0^o$ (b) Mt = 0.30, $\alpha = 10.0^o$ (c) Mt = 0.30, $\alpha = 20.0^o$

(d) Mt = 0.50, $\alpha = 0.0^o$ (e) Mt = 0.50, $\alpha = 10.0^o$ (f) Mt = 0.50, $\alpha = 20.0^o$

(g) Mt = 0.70, $\alpha = 0.0^o$ (h) Mt = 0.70, $\alpha = 10.0^o$ (i) Mt = 0.70, $\alpha = 20.0^o$

Figure (3): Engine face total pressure recovery contours for the baseline inlet S-duct over the mission variable range.

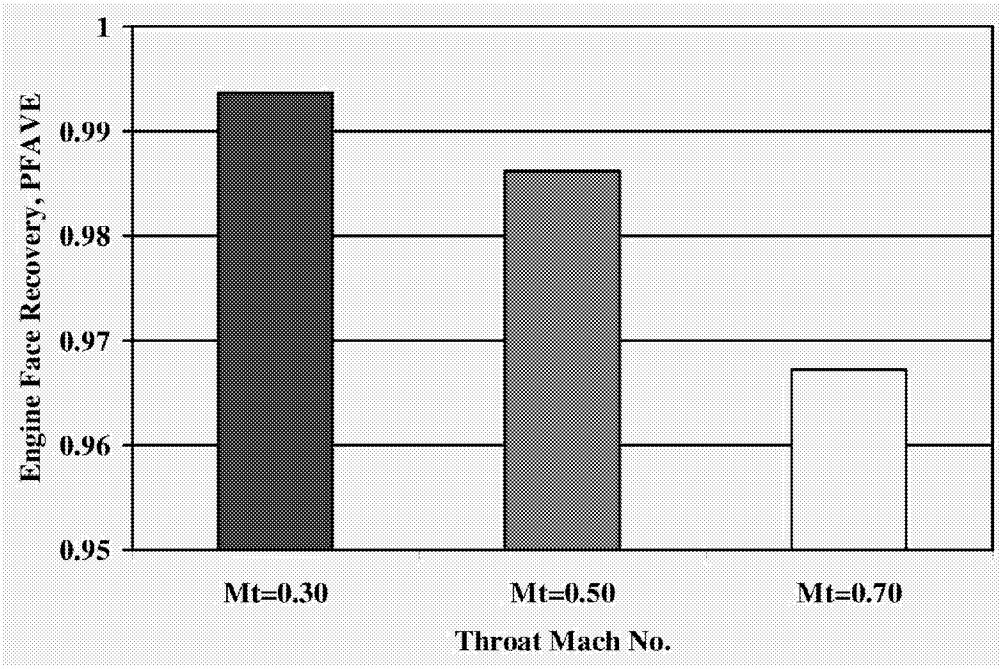

Figure (4): Effect of inlet throat Mach number on the engine face total pressure recovery, baseline inlet S-duct, $\alpha = 0.0^{o}$.

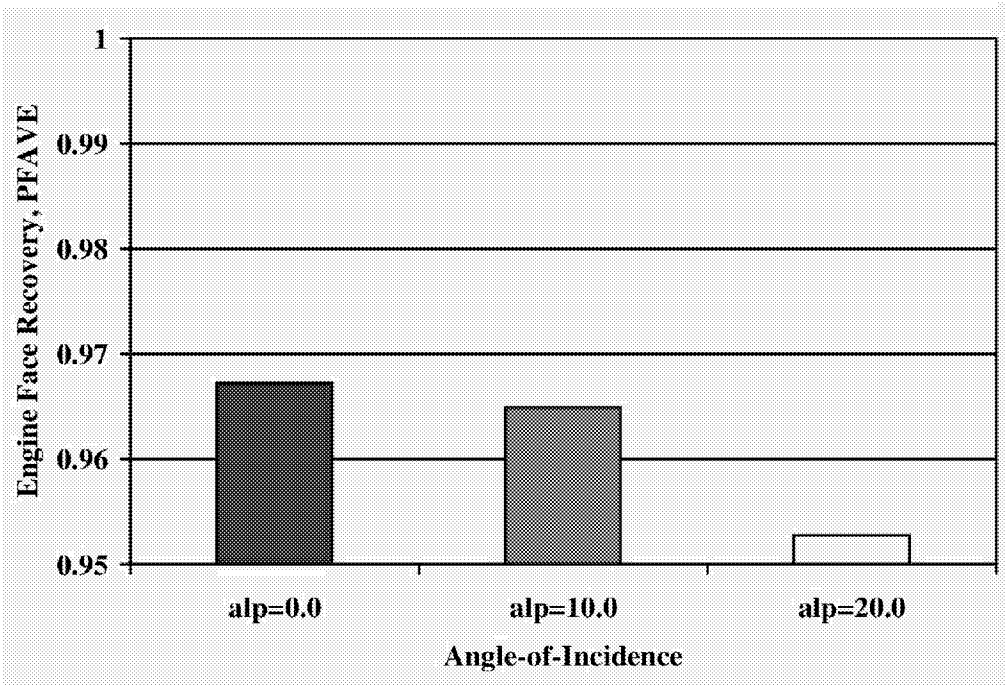

Figure (5): Effect of inlet angle-of-incidence on engine face total pressure recovery, baseline inlet S-duct, Mt = 0.70.

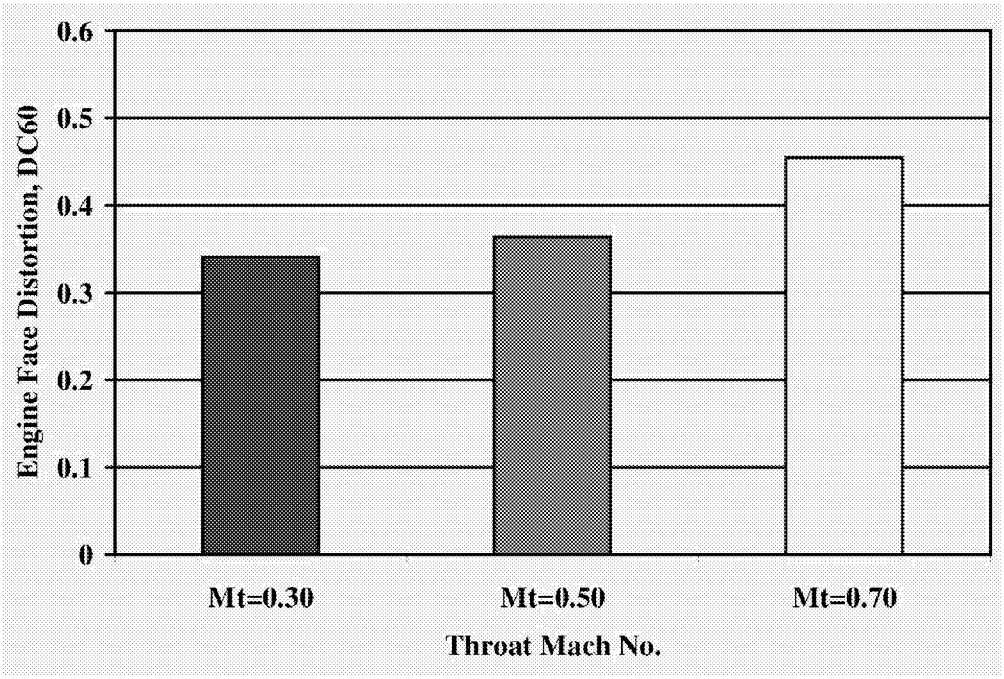

Figure (6): Effect of inlet throat Mach number on the engine face DC60 distortion, baseline inlet S-duct, $\alpha = 0.0^{o}$.

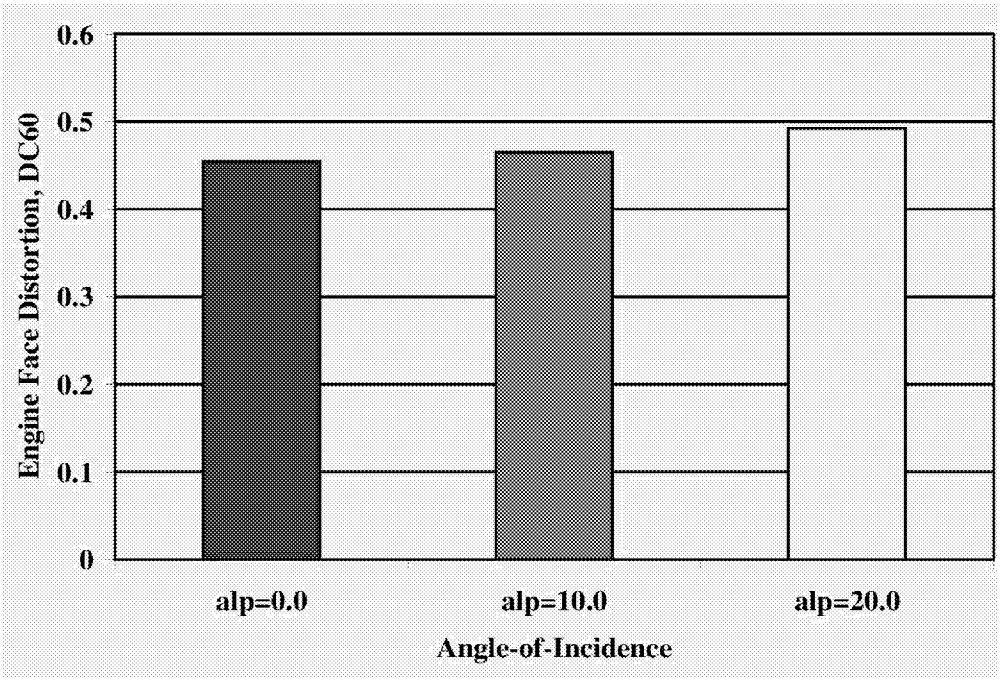

Figure (7): Effect of inlet angle-of-incidence on engine face DC60 distortion, baseline inlet S-duct, Mt = 0.70.

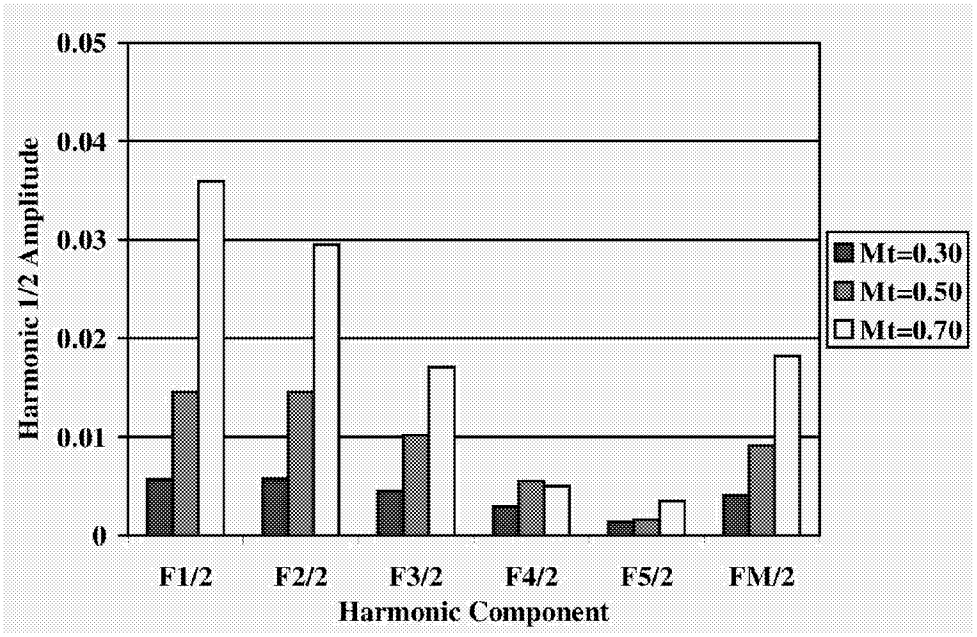

Figure (8): Effect of inlet throat Mach number on the Fourier harmonic 1/2-amplitudes of engine face distortion, baseline inlet S-duct, $\alpha = 0.0^{o}$.

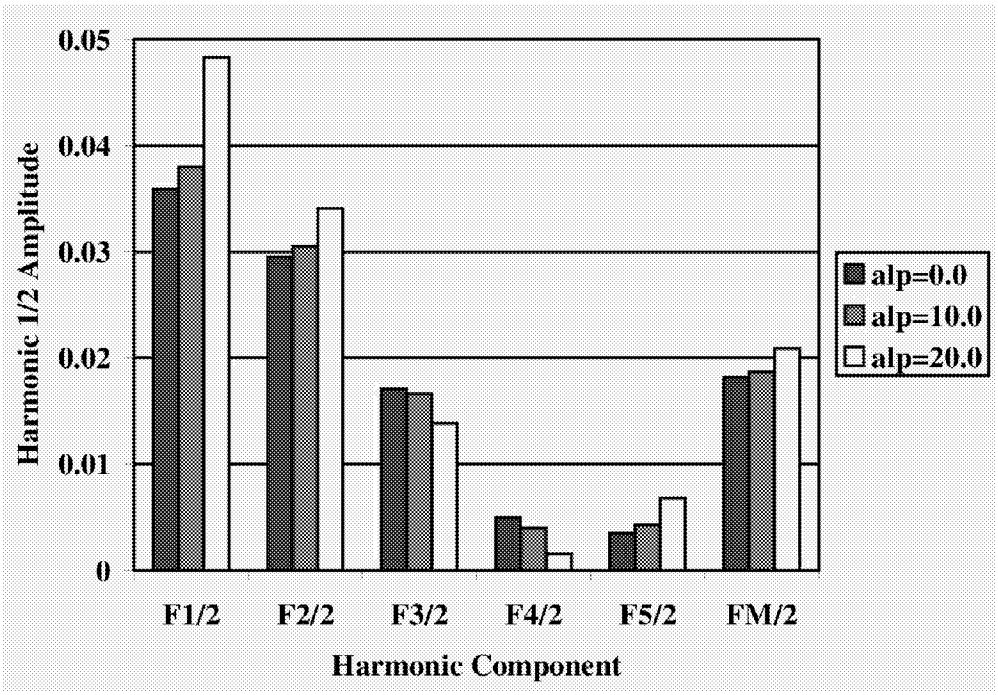

Figure (9): Effect of inlet angle-of-incidence on the Fourier harmonic 1/2-amplitudes of engine face distortion, baseline inlet S-duct, Mt = 0.70.

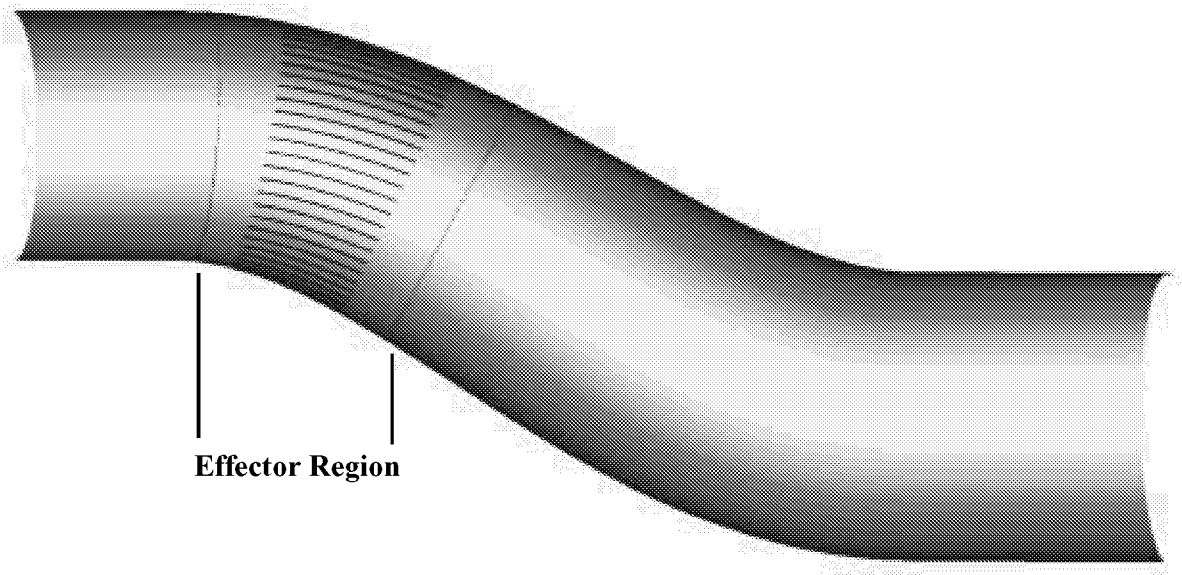

Figure (10): Location of effector region within inlet S-duct configuration.

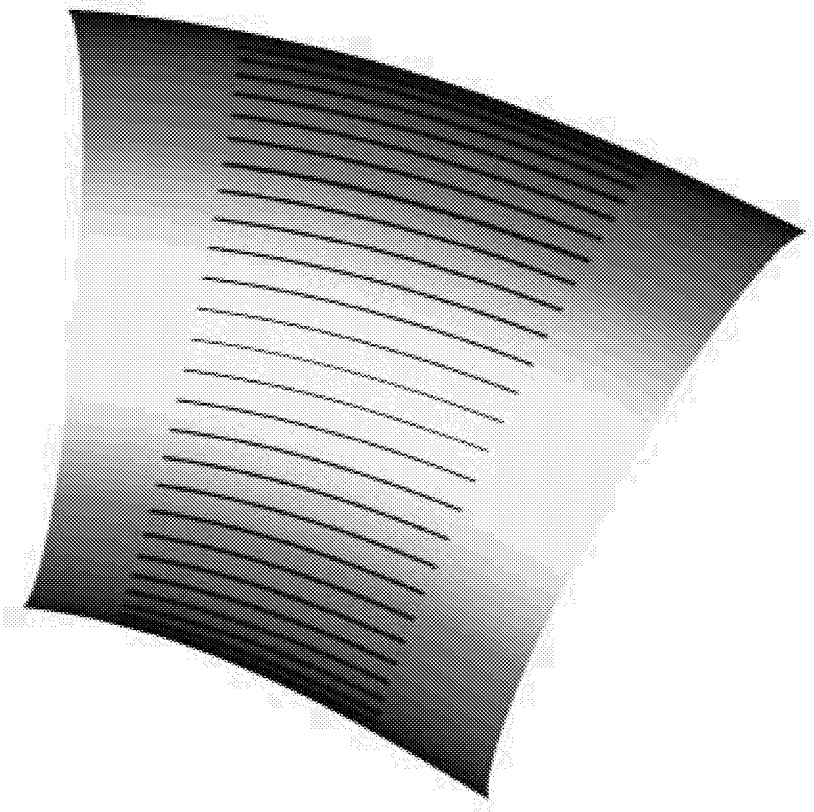

Figure (11): Micro-vane arrangement within inlet S-duct effector region.

Factor	Range
Number of Vane Effectors, n	13 to 27
Effector Vane Height (mm), h	1.0 to 2.0
Effector Chord Length (mm), c	36.0 to 72.0
Inlet Throat Mach Number, Mt	0.30 to 0.70
Inlet Angle-of-Incidence (degs.), α	0.0 to 20.0

Table (3): Factor variables which establish the DOE design matrix.

Variable	Value
Effector Vane Thickness (mm), t	0.138
Vane Angle-of-Incidence (degs), β	5.0
Inlet Total Pressure (lbs/ft^2), Pt	10506.0
Inlet Total Temperature (^{o}R), Tt	517.0
Inlet Angle-of-Yaw (degs), γ	0.0

Table (4): Variables held constant.

Response	Nomenclature
Engine Face Total Pressure Recovery	PFAVE
Engine Face Distortion	DC60
1st Fourier Harmonic 1/2-Amplitude	F1/2
2nd Fourier Harmonic 1/2-Amplitude	F2/2
3rd Fourier Harmonic 1/2-Amplitude	F3/2
4th Fourier Harmonic 1/2-Amplitude	F4/2
5th Fourier Harmonic 1/2-Amplitude	F5/2

Table (5): DOE response variables.

Config.	n	h	c	Mt	α
nvg701	13	1.0	36.0	0.30	20.0
nvg702	27	1.0	36.0	0.30	0.0
nvg703	13	2.0	36.0	0.30	0.0
nvg704	27	2.0	36.0	0.30	20.0
nvg705	13	1.0	72.0	0.30	0.0
nvg706	27	1.0	72.0	0.30	20.0
nvg707	13	2.0	72.0	0.30	20.0
nvg708	27	2.0	72.0	0.30	0.0
nvg709	13	1.0	36.0	0.70	0.0
nvg710	27	1.0	36.0	0.70	20.0
nvg711	13	2.0	36.0	0.70	20.0
nvg712	27	2.0	36.0	0.70	0.0
nvg713	13	1.0	72.0	0.70	20.0
nvg714	27	1.0	72.0	0.70	0.0
nvg715	13	2.0	72.0	0.70	0.0
nvg716	27	2.0	72.0	0.70	20.0
nvg717	13	1.5	54.0	0.50	10.0
nvg718	27	1.5	54.0	0.50	10.0
nvg719	20	1.0	54.0	0.50	10.0
nvg720	20	2.0	54.0	0.50	10.0
nvg721	20	1.5	36.0	0.50	10.0
nvg722	20	1.5	72.0	0.50	10.0
nvg723	20	1.5	54.0	0.30	10.0
nvg724	20	1.5	54.0	0.70	10.0
nvg725	20	1.5	54.0	0.50	0.0
nvg726	20	1.5	54.0	0.50	20.0
nvg727	20	1.5	54.0	0.50	10.0

Table (6): "Lower Order" Central Composite Face-Centered (CCF) combined array DOE format involving factor (design) variables and environmental (mission) variables.

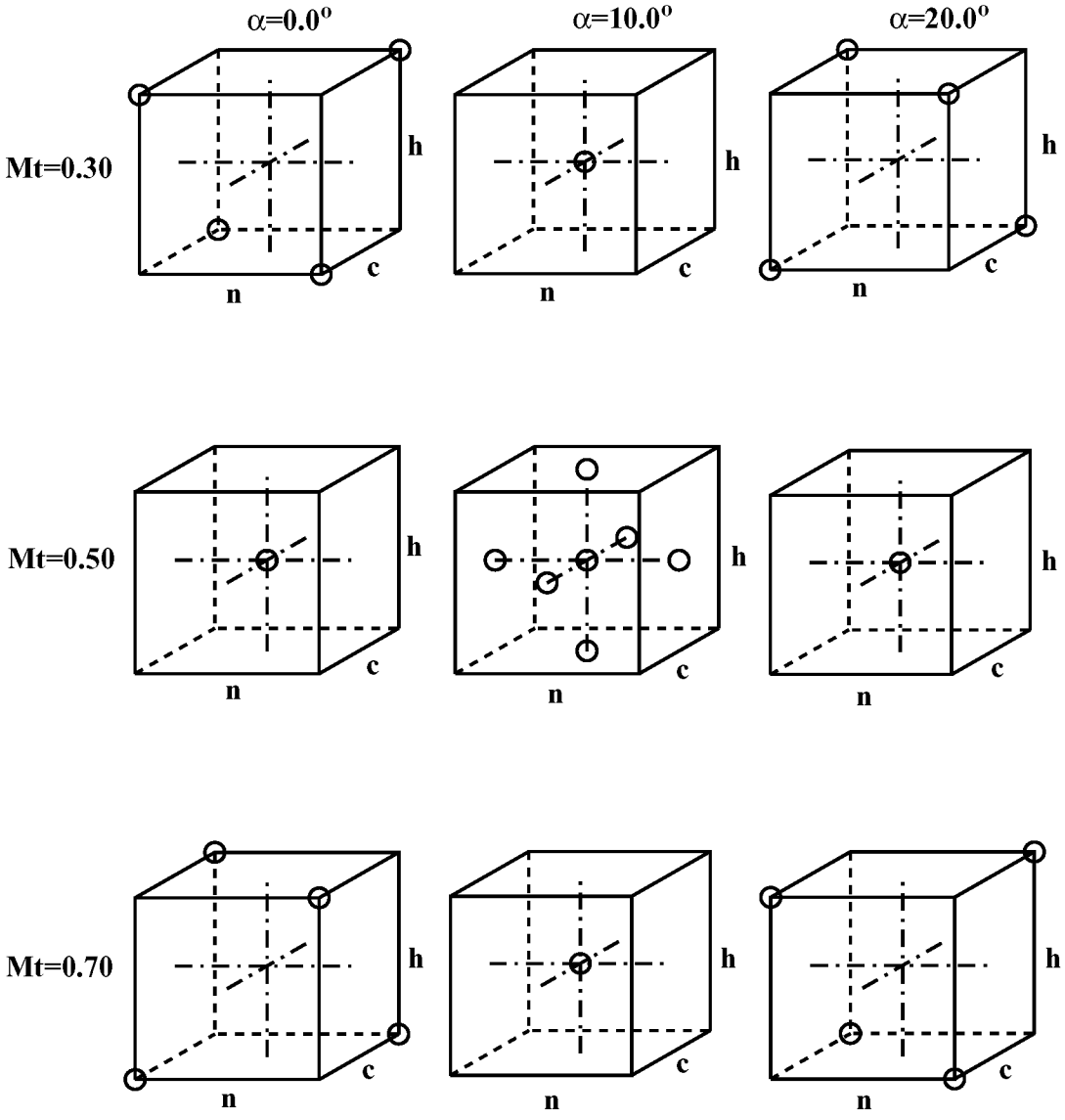

Figure (12): Graphical representation of the "Lower Order" Central Composite Face-Centered (CCF) combined array DOE format involving factor (design) variables and environmental (mission) variables.

Ring Number	Radial Weighting Coefficient
1	0.05651
2	0.14248
3	0.21077
4	0.26918
5	0.32106

Table (7): Radial weighting coefficients applied to the total pressure rake measurements.

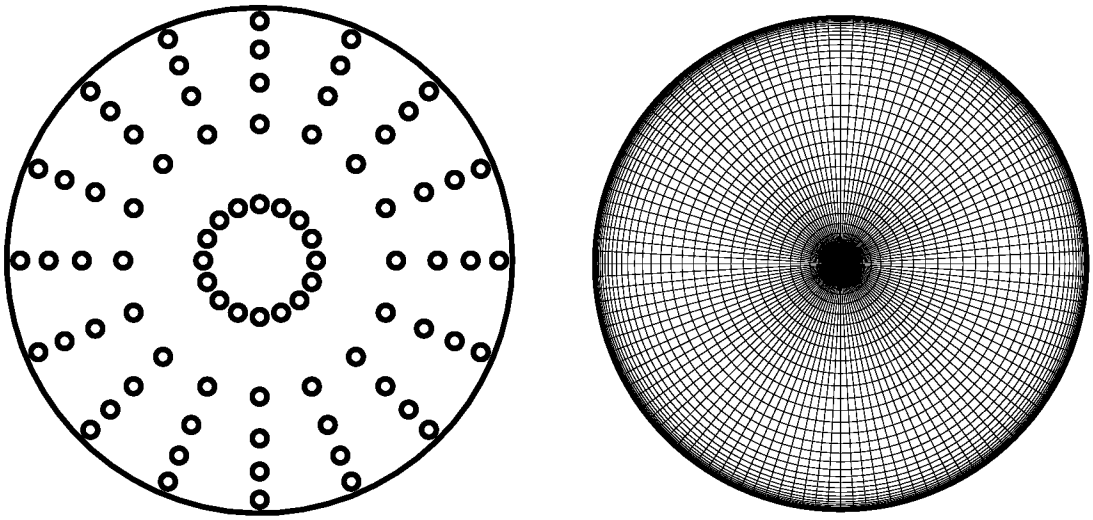

(a) 80-probe rake **(b) Computational grid**

Figure (13): Total pressure and distortion measurement arrays.

Response	Nomenclature	S^2_{max}/S^2_{min}	t(0.95,9,9)
1st Harmonic 1/2-Amplitude	F1/2	1939.9	4.03
2nd Harmonic 1/2-Amplitude	F2/2	391.6	4.03
3rd Harmonic 1/2-Amplitude	F3/2	1681.0	4.03
4th Harmonic 1/2-Amplitude	F4/2	153.9	4.03
5th Harmonic 1/2-Amplitude	F5/2	292.3	4.03

Table (8): Fourier Harmonic 1/2-amplitude F-test compliance

Config.	PFAVE	DC(60)	F1/2	F2/2	F3/2	F4/2	F5/2
nvg701	0.98892	0.07588	0.00067	0.00263	0.00107	0.00052	0.00052
nvg702	0.99460	0.03610	0.00279	0.00155	0.00176	0.00025	0.00022
nvg703	0.99451	0.04464	0.00345	0.00182	0.00140	0.00048	0.00039
nvg704	0.99053	0.03336	0.00320	0.00230	0.00201	0.00077	0.00085
nvg705	0.99498	0.03660	0.00282	0.00152	0.00143	0.00040	0.00012
nvg706	0.99072	0.03273	0.00293	0.00180	0.00200	0.00057	0.00035
nvg707	0.99138	0.04374	0.00369	0.00195	0.00128	0.00073	0.00053
nvg708	0.99489	0.07689	0.00594	0.00286	0.00122	0.00020	0.00065
nvg709	0.97405	0.19080	0.01753	0.01474	0.00622	0.00085	0.00386
nvg710	0.96183	0.24010	0.02856	0.01960	0.00421	0.00442	0.00613
nvg711	0.96431	0.20937	0.02096	0.01503	0.00553	0.00039	0.00423
nvg712	0.97633	0.04567	0.00412	0.01193	0.00858	0.00240	0.00339
nvg713	0.96250	0.27487	0.02827	0.02212	0.00933	0.00043	0.00413
nvg714	0.97727	0.05010	0.00034	0.00910	0.01055	0.00322	0.00121‘
nvg715	0.97850	0.02916	0.00492	0.00842	0.00572	0.00352	0.00288
nvg716	0.96591	0.04687	0.00581	0.00303	0.00606	0.00484	0.00701
nvg717	0.98674	0.01487	0.00148	0.00242	0.00285	0.00147	0.00098
nvg718	0.98665	0.03322	0.00485	0.00539	0.00441	0.00095	0.00121
nvg719	0.98636	0.02689	0.00097	0.00243	0.00429	0.00201	0.00040
nvg720	0.98646	0.03927	0.00643	0.00581	0.00309	0.00072	0.00138
nvg721	0.98647	0.02511	0.00232	0.00371	0.00392	0.00108	0.00047
nvg722	0.98703	0.03559	0.00580	0.00538	0.00340	0.00057	0.00107
nvg723	0.99309	0.04708	0.00391	0.00228	0.00150	0.00028	0.00037
nvg724	0.97462	0.04156	0.00031	0.00891	0.00843	0.00257	0.00172
nvg725	0.98807	0.03531	0.00503	0.00536	0.00358	0.00060	0.00069
nvg726	0.98277	0.02139	0.00138	0.00305	0.00355	0.00131	0.00100
nvg727	0.98684	0.02975	0.00416	0.00478	0.00374	0.00085	0.00073

Table (9): Engine face performance results for the Central Composite Face-Centered (CCF) combined array DOE format involving design (factor) variables and mission (environmental) variables.

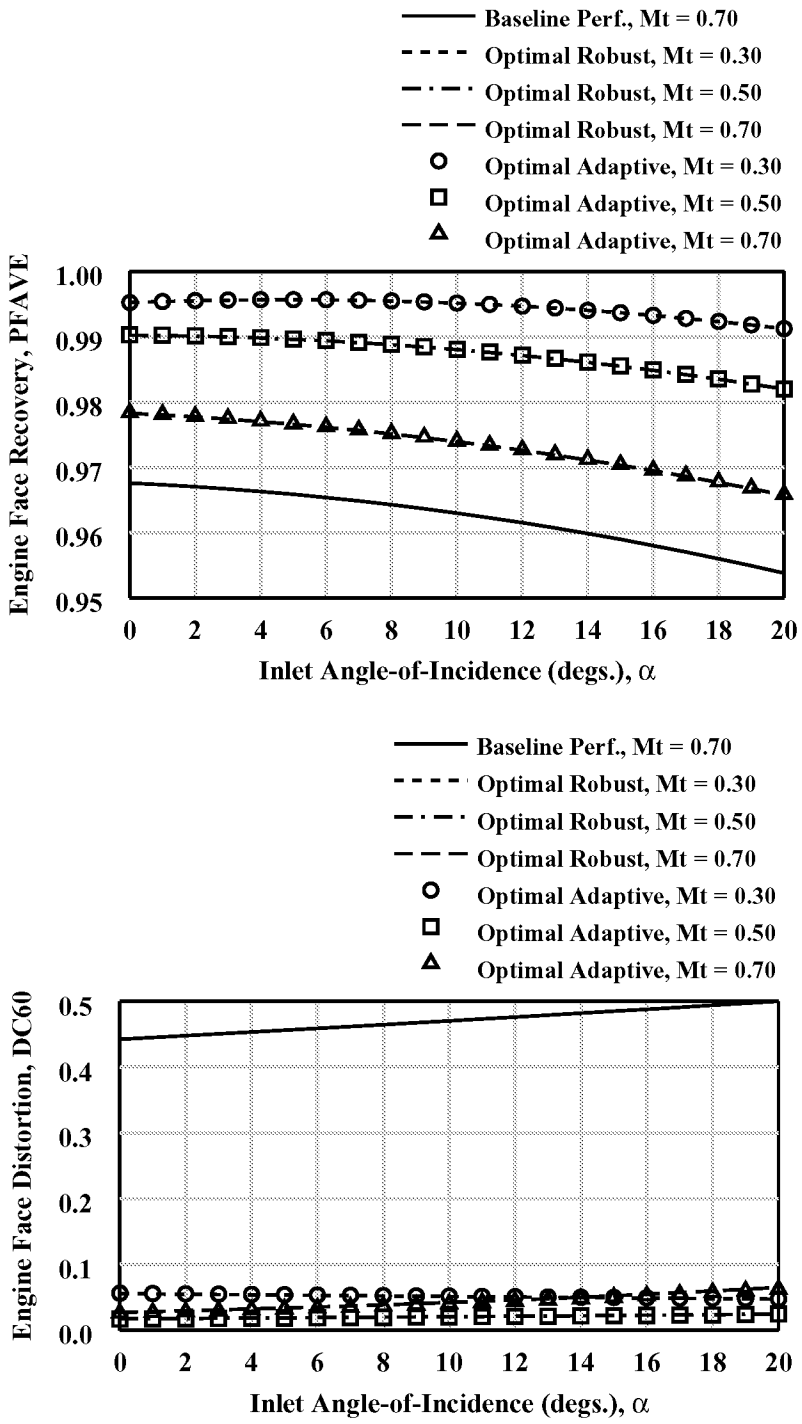

Figure (14): Comparison of "Optimal Robust" and "Optimal Adaptive" Maximum Performance inlet mission installation designs.

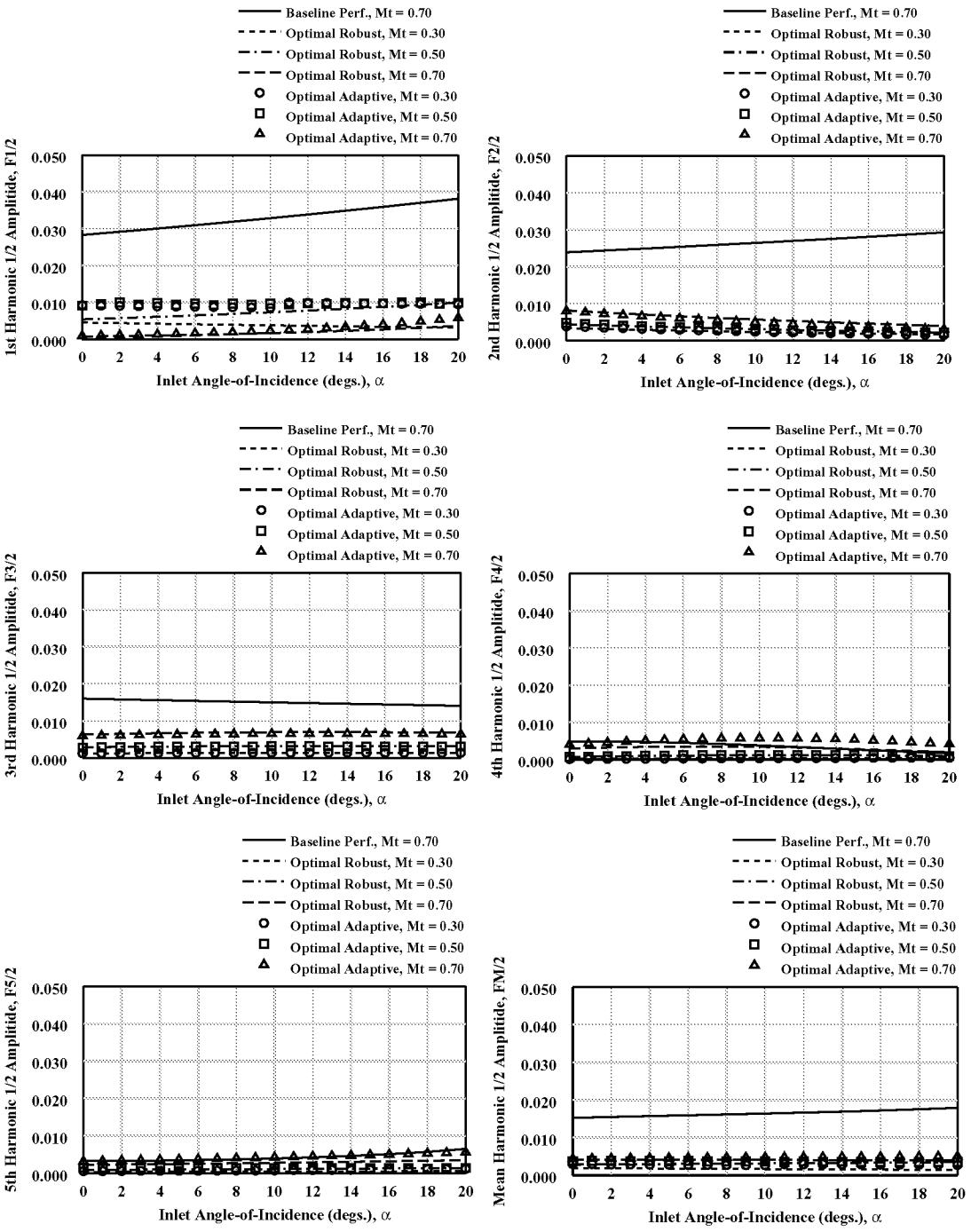

Figure (14): Comparison of "Optimal Robust" and "Optimal Adaptive" Maximum Performance inlet mission installation designs, continued.

Config.	n	h	c	Mt	α
nvg728	22	1.95	72.0	0.70	0.0
nvg729	22	1.95	72.0	0.70	10.0
nvg730	22	1.95	72.0	0.70	20.0
nvg731	22	1.95	72.0	0.50	0.0
nvg732	22	1.95	72.0	0.50	10.0
nvg733	22	1.95	72.0	0.50	20.0
nvg734	22	1.95	72.0	0.30	0.0
nvg735	22	1.95	72.0	0.30	10.0
nvg736	22	1.95	72.0	0.30	20.0

Table (10): "Optimal Robust" Maximum Performance inlet mission CFD validation cases.

Config.	PFAVE	DC(60)	F1/2	F2/2	F3/2	F4/2	F5/2
nvg728	0.97803	0.04904	0.01070	0.01262	0.00543	0.00104	0.00289
nvg729	0.97585	0.02144	0.00289	0.00392	0.00383	0.00200	0.00194
nvg730	0.96629	0.04842	0.00634	0.00190	0.00431	0.00473	0.00777
nvg731	0.98835	0.04936	0.00867	0.00629	0.00295	0.00057	0.00124
nvg732	0.98722	0.04412	0.00804	0.00610	0.00329	0.00080	0.00129
nvg733	0.98304	0.02739	0.00533	0.00502	0.00374	0.00168	0.00201
nvg734	0.99432	0.07512	0.00587	0.00288	0.00117	0.00030	0.00066
nvg735	0.99337	0.07170	0.00566	0.00275	0.00134	0.00034	0.00061
nvg736	0.99081	0.05397	0.00468	0.00250	0.00154	0.00054	0.00068

Table (11): "Optimal Robust" Maximum Performance inlet mission CFD validation results.

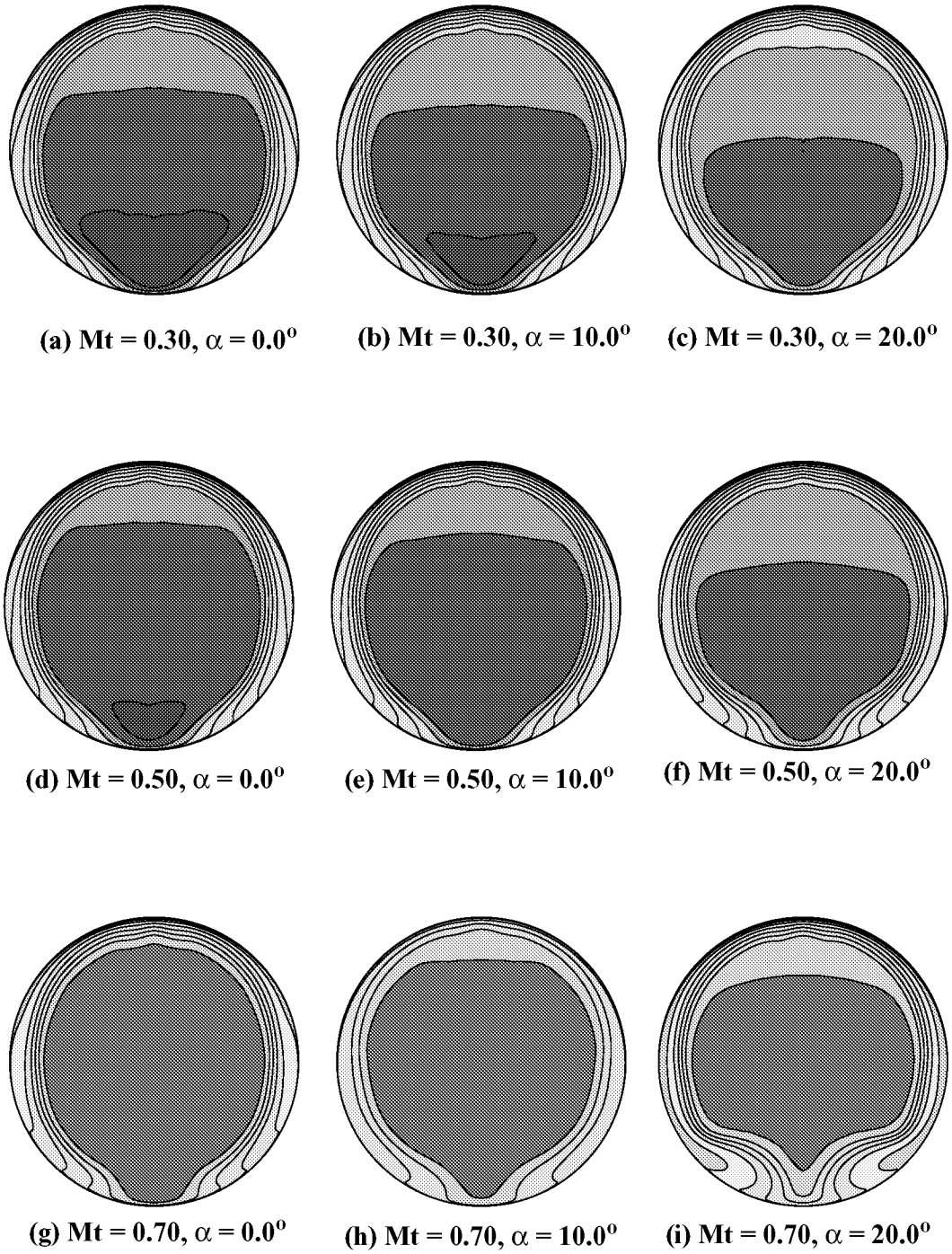

(a) Mt = 0.30, $\alpha = 0.0^o$ (b) Mt = 0.30, $\alpha = 10.0^o$ (c) Mt = 0.30, $\alpha = 20.0^o$

(d) Mt = 0.50, $\alpha = 0.0^o$ (e) Mt = 0.50, $\alpha = 10.0^o$ (f) Mt = 0.50, $\alpha = 20.0^o$

(g) Mt = 0.70, $\alpha = 0.0^o$ (h) Mt = 0.70, $\alpha = 10.0^o$ (i) Mt = 0.70, $\alpha = 20.0^o$

Figure (15): Engine face total pressure recovery contours for the "Optimal Robust" Maximum Performance inlet mission installation CFD solutions.

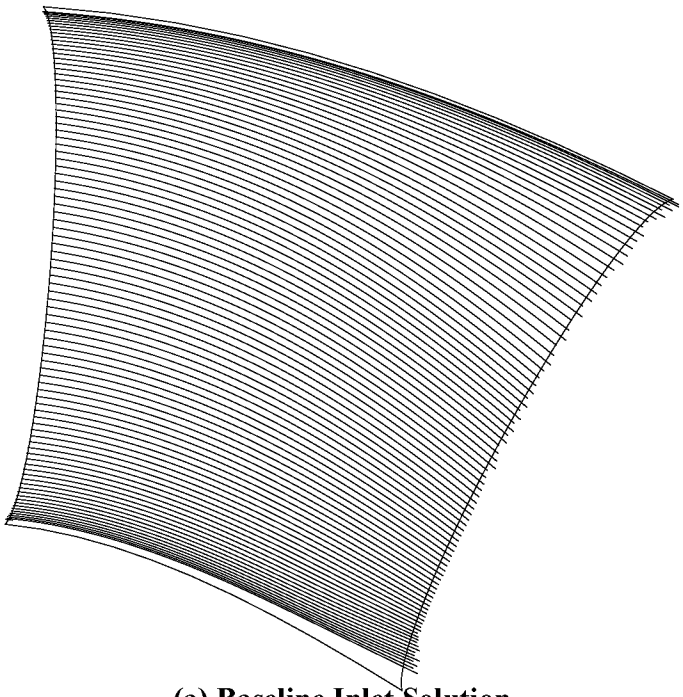

(a) Baseline Inlet Solution

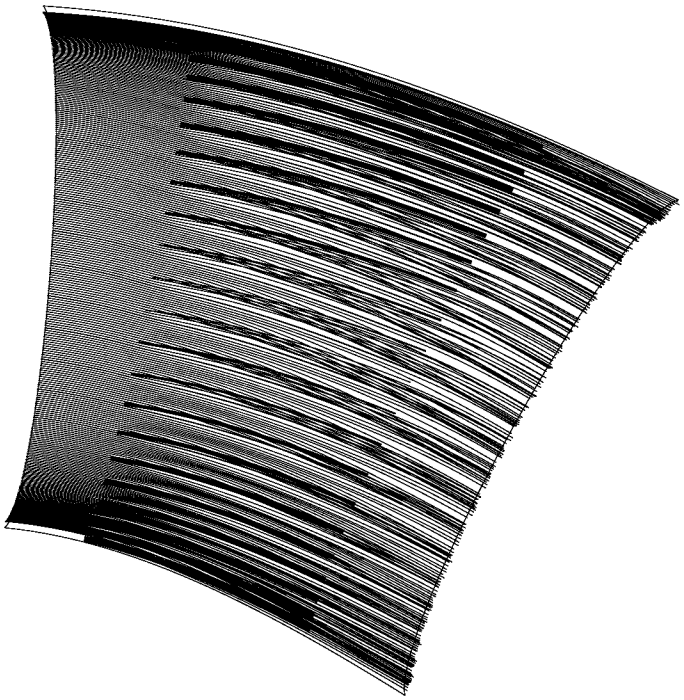

(b) Optimal Robust "Maximum Performance" solution

Figure (16): Comparison of near wall streamlines for baseline and "Optimal Robust" Maximum Performance installation CFD solution, Mt = 0.30, $\alpha = 0.0^{o}$.

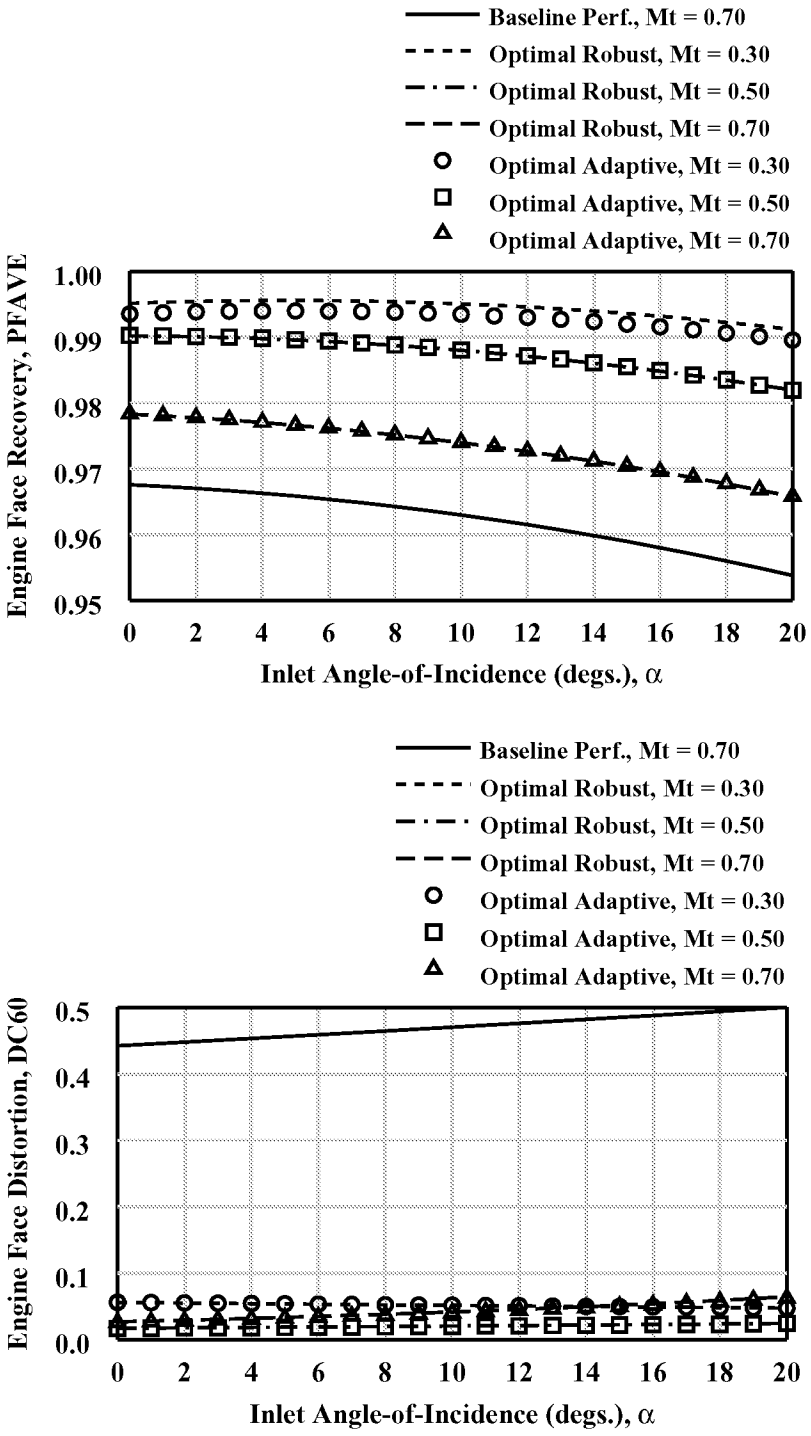

Figure (17): Comparison of "Optimal Robust" and "Optimal Adaptive" Maximum Engine Stability inlet mission installation designs.

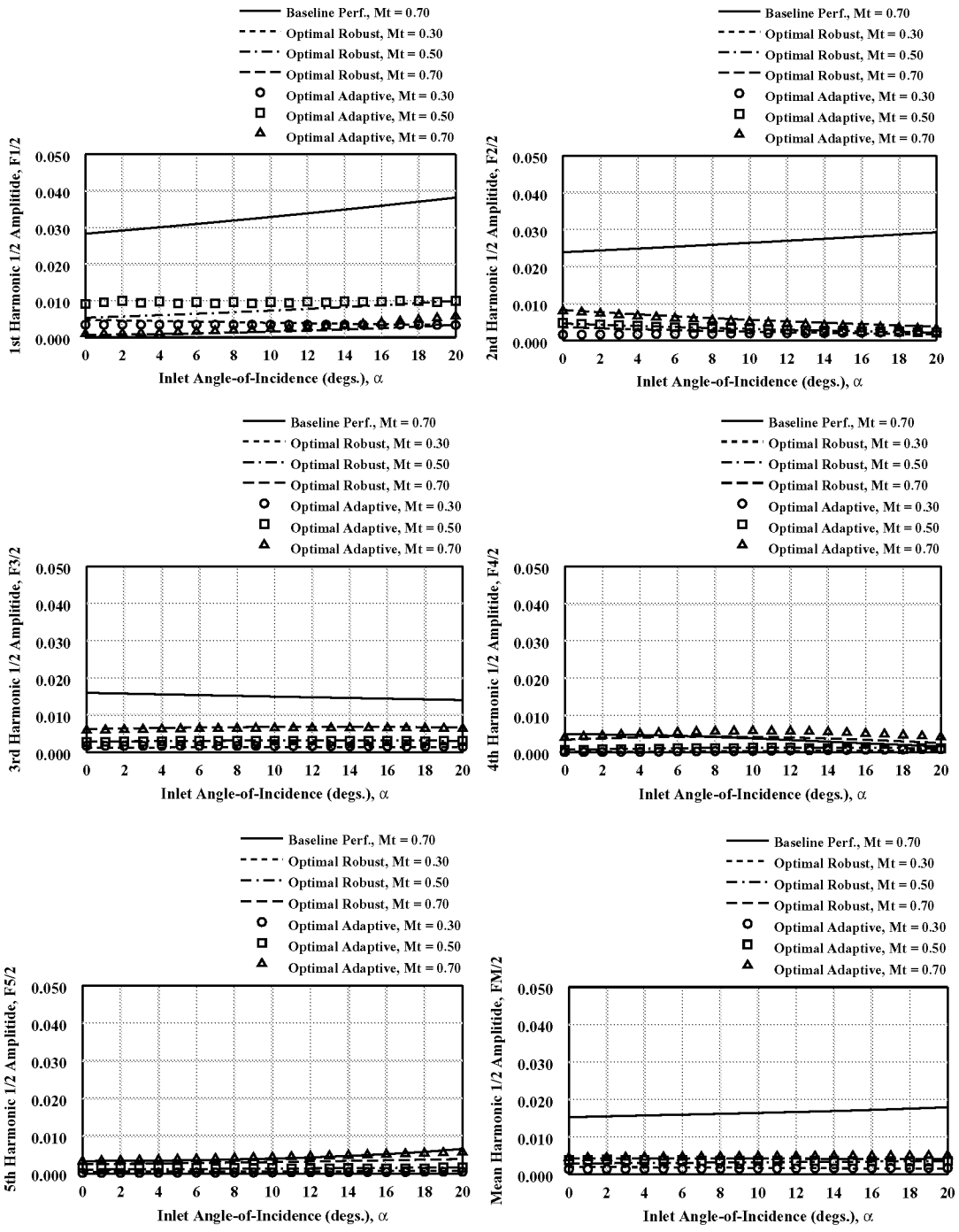

Figure (17): Comparison of "Optimal Robust" and "Optimal Adaptive" Maximum Engine Stability inlet mission installation designs, continued.

Config.	n	h	c	Mt	α
nvg737	24	2.0	70.2	0.70	0.0
nvg738	24	2.0	70.2	0.70	10.0
nvg739	24	2.0	70.2	0.70	20.0
nvg740	24	2.0	70.2	0.50	0.0
nvg741	24	2.0	70.2	0.50	10.0
nvg742	24	2.0	70.2	0.50	20.0
nvg743	24	2.0	70.2	0.30	0.0
nvg744	24	2.0	70.2	0.30	10.0
nvg745	24	2.0	70.2	0.30	20.0

Table (12): "Optimal Robust" Maximum Engine Stability inlet mission CFD validation cases.

Config.	PFAVE	DC(60)	F1/2	F2/2	F3/2	F4/2	F5/2
nvg737	0.97784	0.05082	0.01110	0.01303	0.00570	0.00074	0.00287
nvg738	0.97576	0.04369	0.00896	0.01219	0.00648	0.00149	0.00328
nvg739	0.96619	0.04643	0.00571	0.00304	0.00557	0.00491	0.00738
nvg740	0.98835	0.05149	0.00899	0.00638	0.00290	0.00030	0.00124
nvg741	0.98722	0.04643	0.00835	0.00623	0.00326	0.00052	0.00129
nvg742	0.98305	0.03018	0.00575	0.00537	0.00387	0.00135	0.00177
nvg743	0.99871	0.07797	0.00603	0.00208	0.00114	0.00017	0.00065
nvg744	0.99337	0.07384	0.00583	0.00278	0.00129	0.00020	0.00061
nvg745	0.99081	0.05620	0.00486	0.00258	0.00154	0.00041	0.00063

Table (13): "Optimal Robust" Maximum Engine Stability inlet mission CFD validation results.

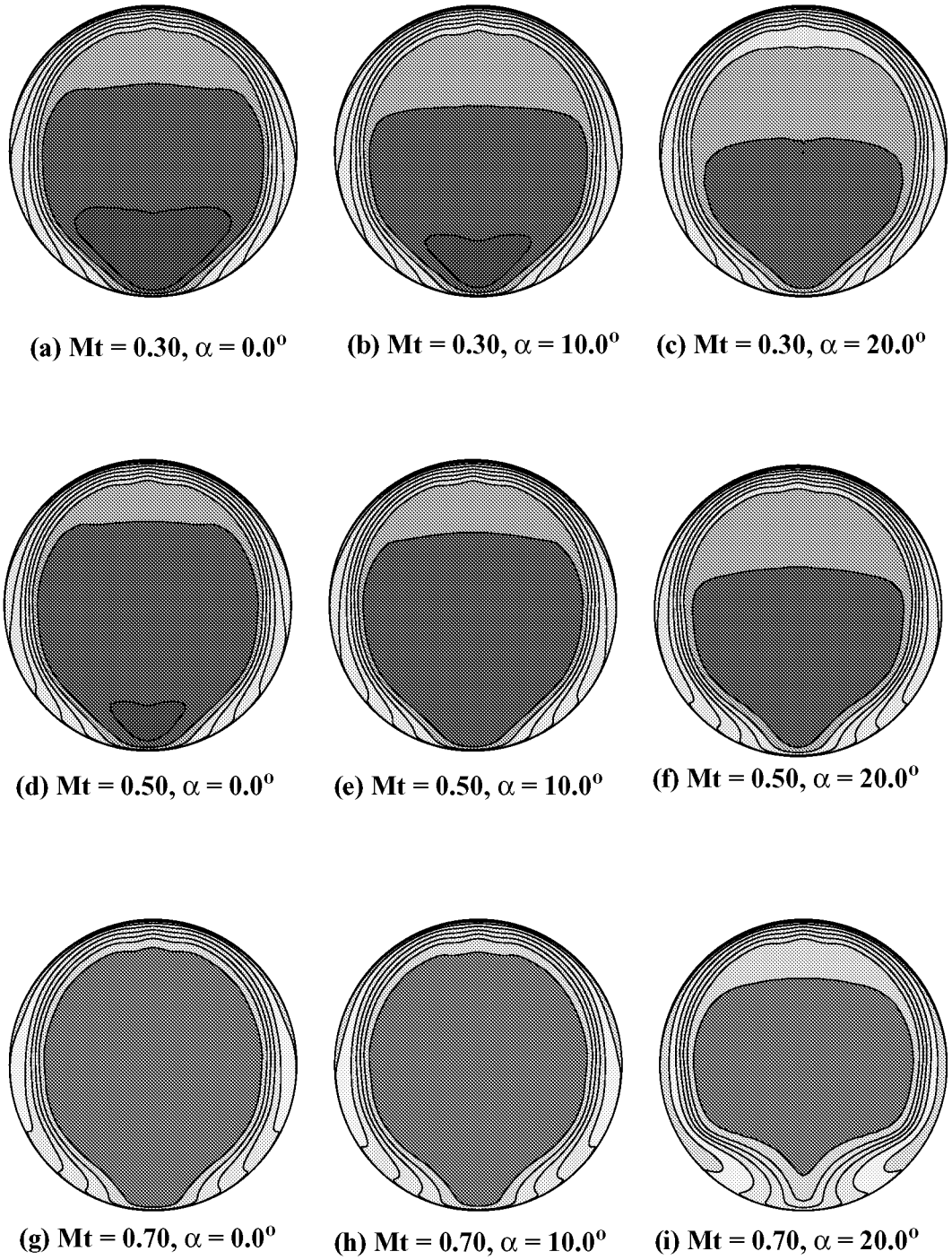

(a) Mt = 0.30, $\alpha = 0.0^o$ (b) Mt = 0.30, $\alpha = 10.0^o$ (c) Mt = 0.30, $\alpha = 20.0^o$

(d) Mt = 0.50, $\alpha = 0.0^o$ (e) Mt = 0.50, $\alpha = 10.0^o$ (f) Mt = 0.50, $\alpha = 20.0^o$

(g) Mt = 0.70, $\alpha = 0.0^o$ (h) Mt = 0.70, $\alpha = 10.0^o$ (i) Mt = 0.70, $\alpha = 20.0^o$

Figure (18): Engine face total pressure recovery contours for the "Optimal Robust" Maximum Engine Stability inlet mission installation CFD solutions.

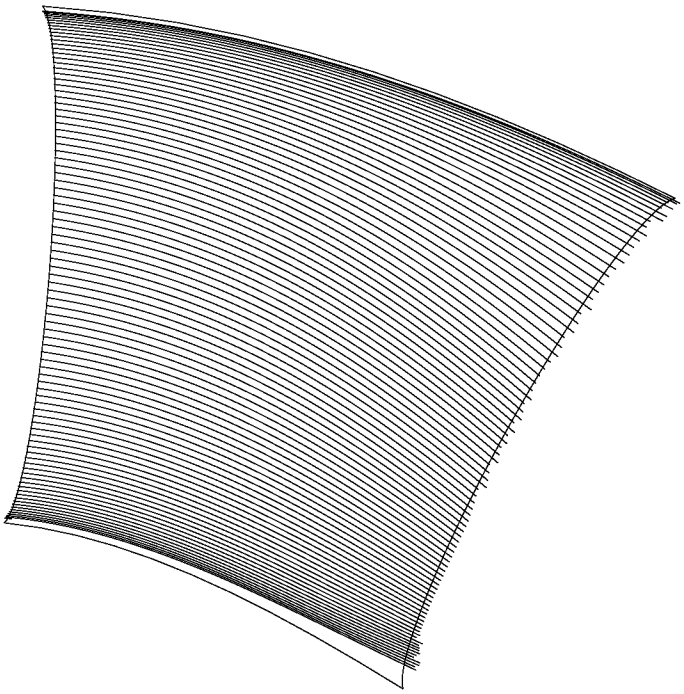

(a) Baseline Inlet Solution

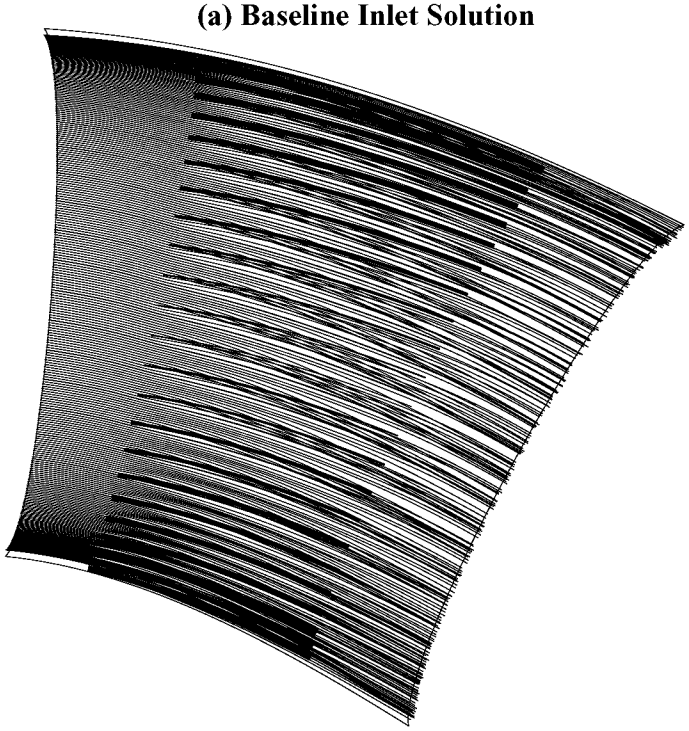

(b) Optimal Robust "Maximum Engine Stability"solution

Figure (19): Comparison of near wall streamlines for baseline and "Optimal Robust" Maximum Engine Stability installation CFD solutions, Mt = 0.50, $\alpha = 10.0^{o}$.

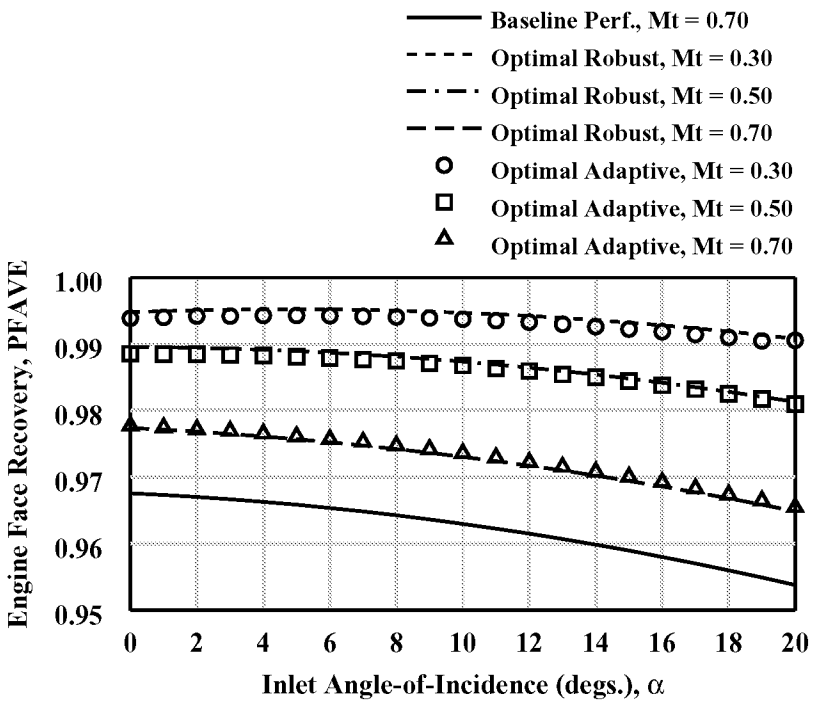

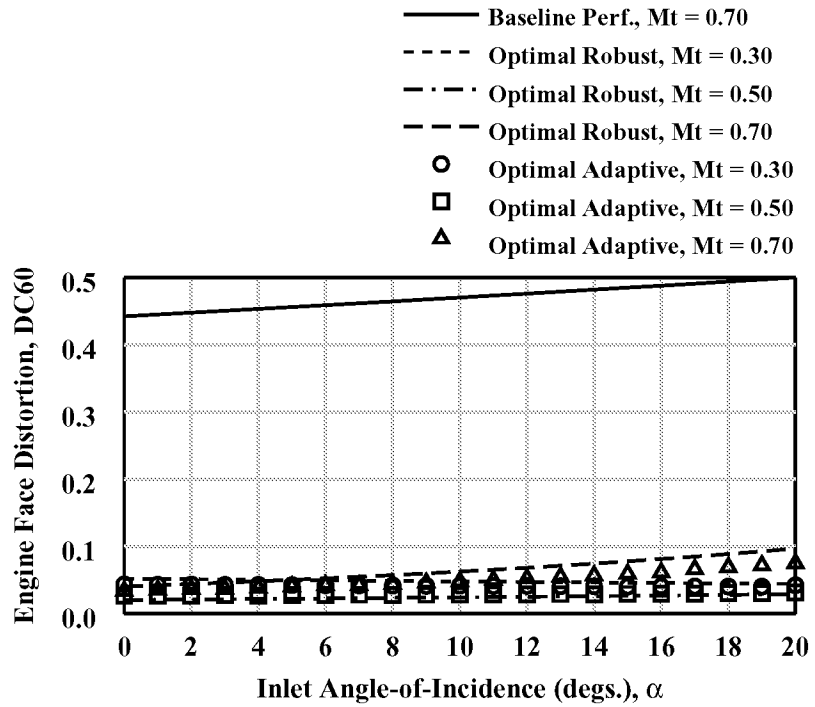

Figure (20): Comparison of "Optimal Robust" and "Optimal Adaptive" Maximum HCF Life Expectancy inlet mission installation designs.

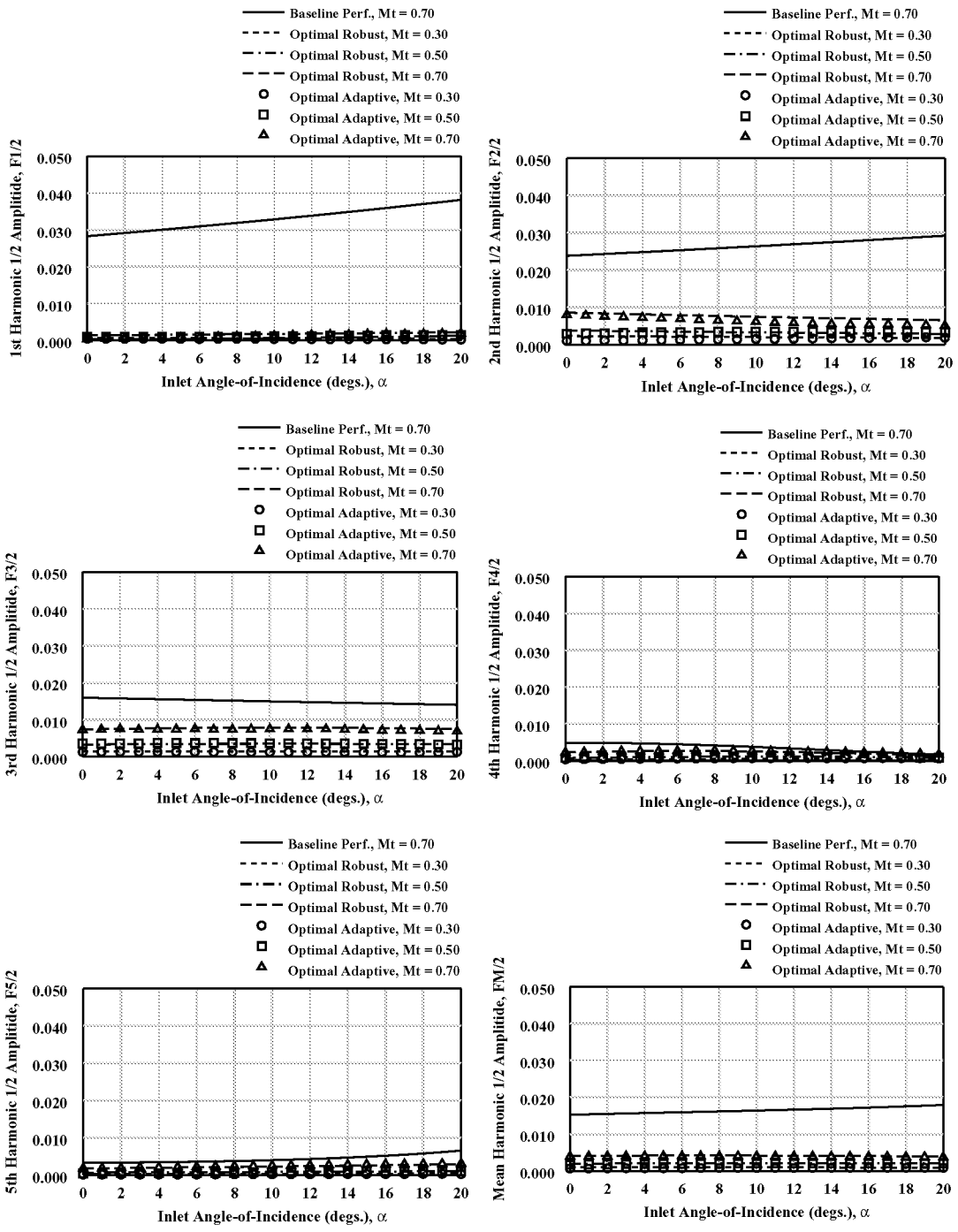

Figure (20): Comparison of "Optimal Robust" and "Optimal Adaptive" Maximum HCF Life Expectancy inlet mission installation designs, continued.

Config.	n	h	c	Mt	α
nvg746	19	1.70	63.0	0.70	0.0
nvg747	19	1.70	63.0	0.70	10.0
nvg748	19	1.70	63.0	0.70	20.0
nvg749	19	1.70	63.0	0.50	0.0
nvg750	19	1.70	63.0	0.50	10.0
nvg751	19	1.70	63.0	0.50	20.0
nvg752	19	1.70	63.0	0.30	0.0
nvg753	19	1.70	63.0	0.30	10.0
nvg754	19	1.70	63.0	0.30	20.0

Table (14): "Optimal Robust" Maximum HCF Life Expectancy inlet mission CFD validation cases.

Config.	PFAVE	DC(60)	F1/2	F2/2	F3/2	F4/2	F5/2
nvg746	0.97813	0.04366	0.00631	0.01173	0.00647	0.00124	0.00238
nvg747	0.97585	0.03636	0.00374	0.01040	0.00688	0.00204	0.00290
nvg748	0.96591	0.07454	0.01207	0.00299	0.00231	0.00331	0.00586
nvg749	0.98864	0.03958	0.00653	0.00588	0.00355	0.00097	0.00119
nvg750	0.98740	0.03481	0.00589	0.00555	0.00376	0.00121	0.00126
nvg751	0.98323	0.02144	0.00289	0.00392	0.00383	0.00200	0.00194
nvg752	0.99470	0.06192	0.00490	0.00279	0.00148	0.00048	0.00061
nvg753	0.99356	0.05861	0.00469	0.00262	0.00162	0.00055	0.00058
nvg754	0.99091	0.04134	0.00365	0.00224	0.00174	0.00071	0.00063

Table (15): "Optimal Robust" Maximum HCF Life Expectancy inlet mission CFD validation results.

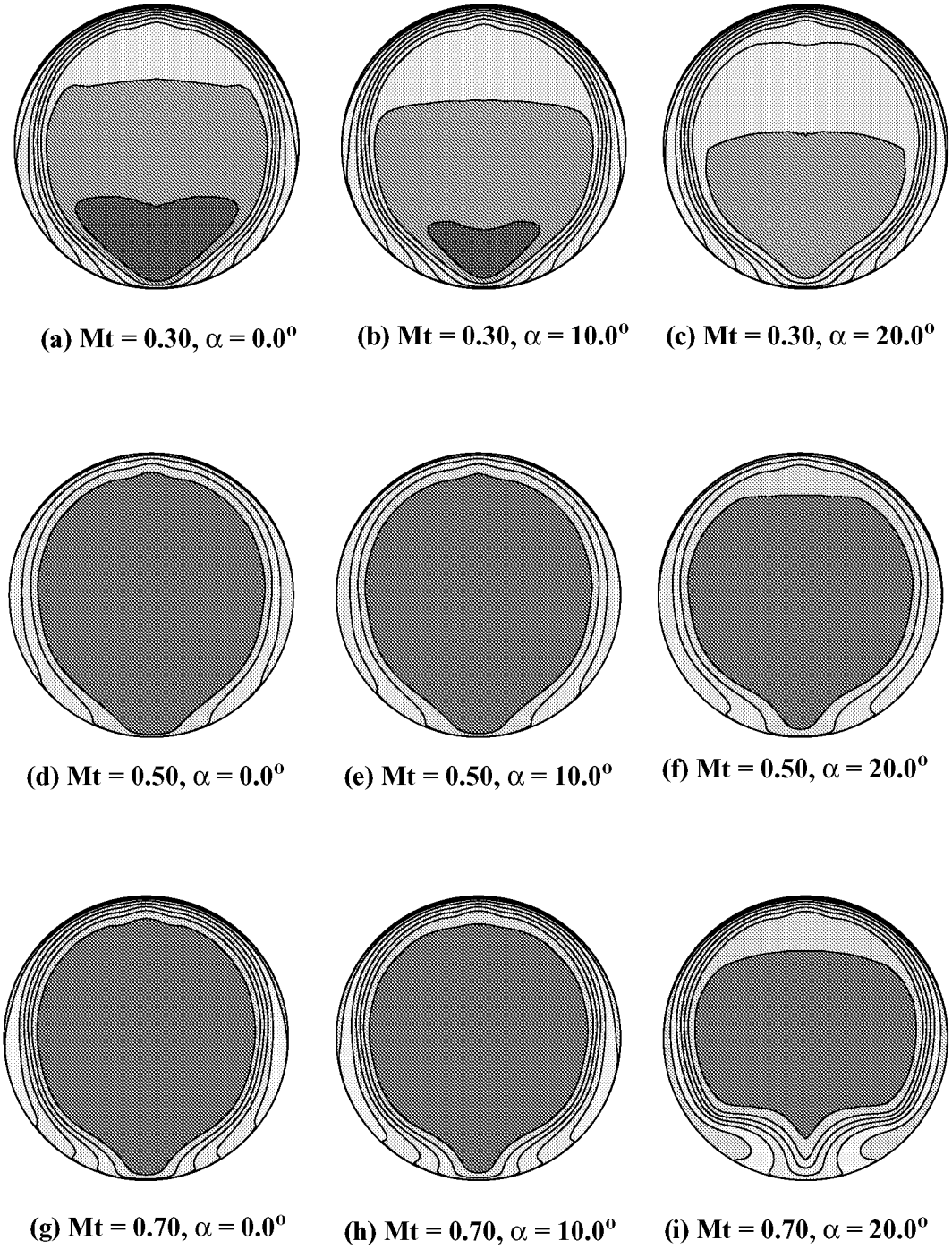

(a) Mt = 0.30, $\alpha = 0.0^o$ (b) Mt = 0.30, $\alpha = 10.0^o$ (c) Mt = 0.30, $\alpha = 20.0^o$

(d) Mt = 0.50, $\alpha = 0.0^o$ (e) Mt = 0.50, $\alpha = 10.0^o$ (f) Mt = 0.50, $\alpha = 20.0^o$

(g) Mt = 0.70, $\alpha = 0.0^o$ (h) Mt = 0.70, $\alpha = 10.0^o$ (i) Mt = 0.70, $\alpha = 20.0^o$

Figure (21): Engine face total pressure recovery contours for the "Optimal Robust" Maximum HCF Life Expectancy inlet mission installation CFD solutions.

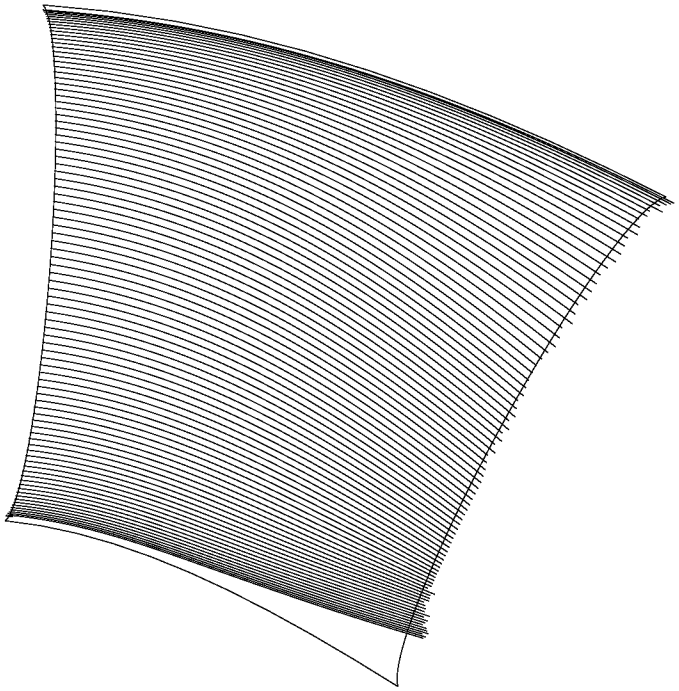

(a) Baseline Inlet Solution

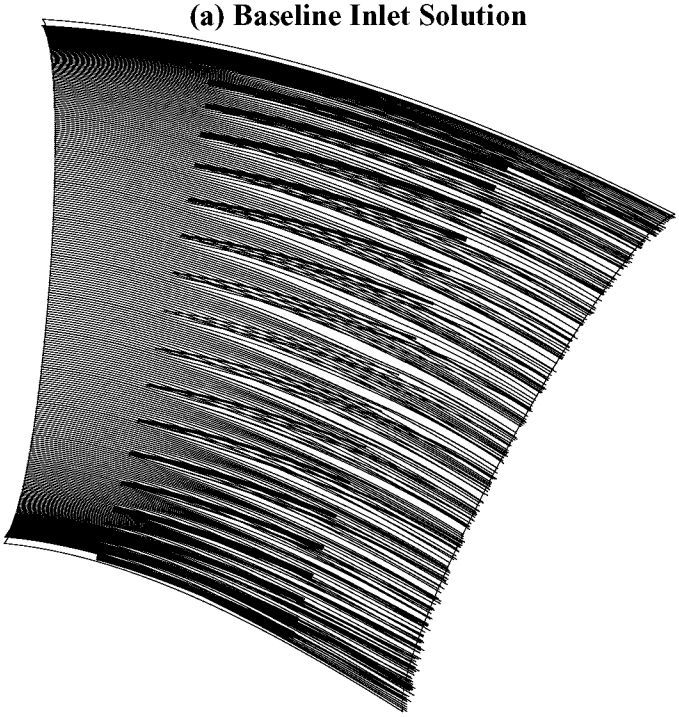

(b) "Optimal Robust" Maximum HCF Life Expectancy solution

Figure (22): Comparison of near wall streamlines for baseline and "Optimal Robust" Maximum HCF Life Expectancy installation CFD solutions, Mt = 0.70, $\alpha = 20.0^{o}$.

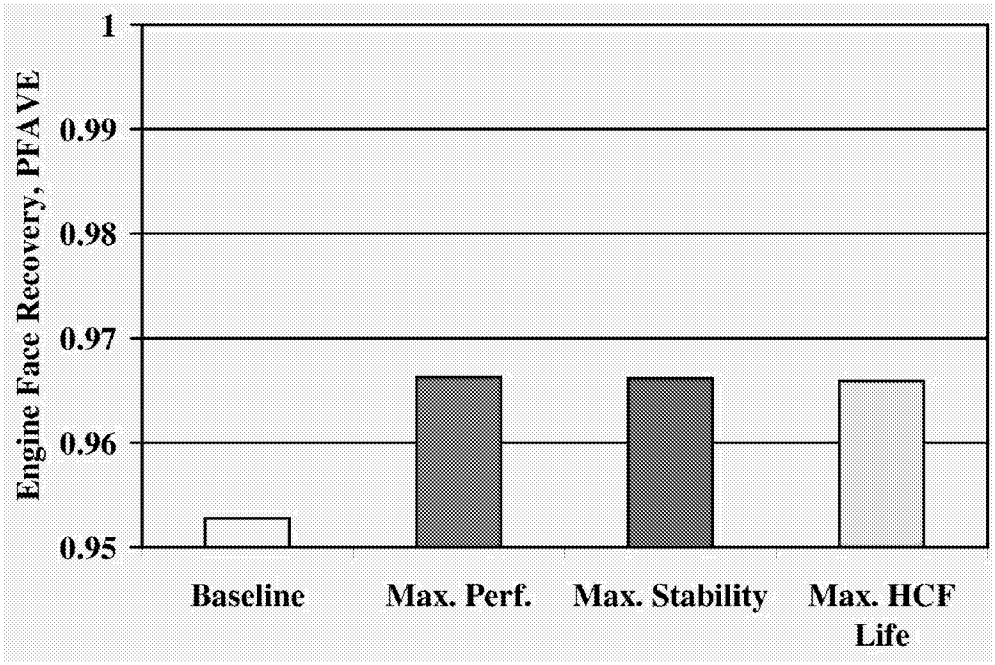

Figure (23): Effect of "Optimal Robust" installation designs on total pressure recovery, Mt = 0.70, α = 20.0^{o}.

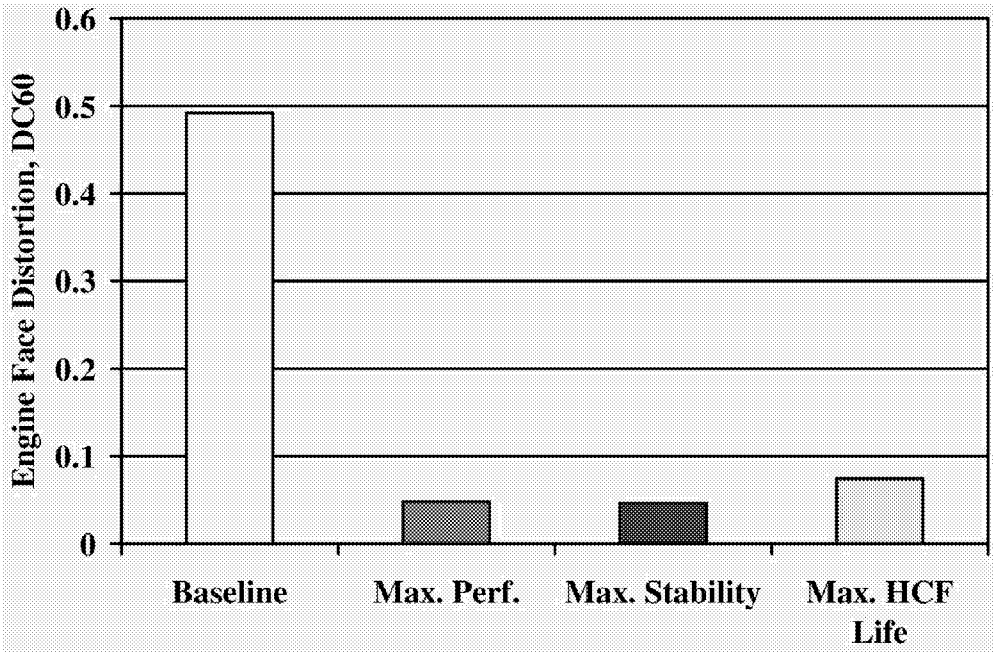

Figure (24): Effect of "Optimal Robust" installation designs on engine face DC60 distortion, Mt = 0.70, α = 20.0^{o}.

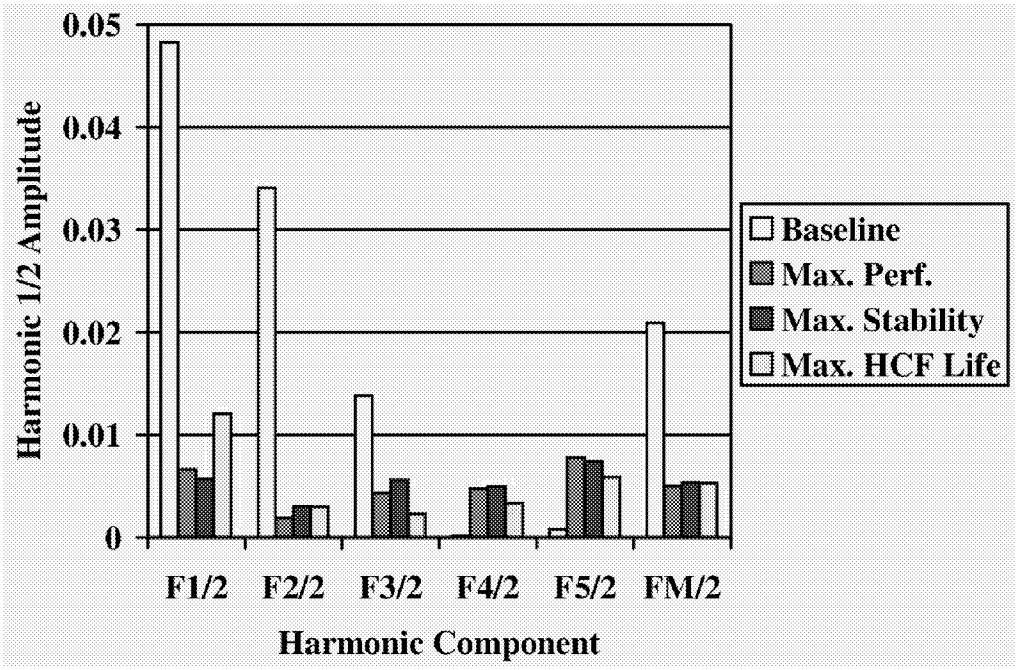

Figure (25): Effect of "Optimal Robust" installation designs on the Fourier harmonic 1/2-amplitudes of engine face distortion, Mt = 0.70, $\alpha = 20.0^{o}$.

Response	$\overline{\ln(Y_1)}$	$\overline{\ln(Y_2)}$	t*	t(0.975,16)	Comment
PFAVE	0.983311	0.984589	0.274126	2.120	Not Diff.
DC60	-3.104553	-2.972547	0.880060	2.120	Not Diff.
F1/2	-5.070342	-4.957721	0.773155	2.120	Not Diff.
F2/2	-5.423593	-5.288741	0.461401	2.120	Not Diff.
F3/2	-5.840606	-5.799162	0.144458	2.120	Not Diff.
F4/2	-6.940625	-7.367960	0.867452	2.120	Not Diff.
F5/2	-6.403719	-6.475028	0.177812	2.120	Not Diff.
FM/2	-5.644880	-5.604631	0.191506	2.120	Not Diff.

Table (16): Statistical comparison of the mean between "Optimal Robust" Maximum Performance (data set 1) and Maximum Engine Stability (data set 2) installation CFD results.

Response	S_1	S_2	F*	F(0.975,8,8)	Comment
PFAVE	0.009538	0.010004	1.048857	4.43	Not Diff.
DC60	0.430507	0.283570	1.386064	4.43	Not Diff.
F1/2	0.395277	0.281970	1.401939	4.43	Not Diff.
F2/2	0.595343	0.628281	1.139752	4.43	Not Diff.
F3/2	0.551444	0.628052	1.138923	4.43	Not Diff.
F4/2	0.936279	1.082130	1.155777	4.43	Not Diff.
F5/2	0.823936	0.859715	1.043424	4.43	Not Diff.
FM/2	0.386132	0.466342	1.207726	4.43	Not Diff.

Table (17): Statistical comparison of the standard deviation between "Optimal Robust" Maximum Performance (data set 1) and Maximum Engine Stability (data set 2) installation CFD results.

Response	$\overline{\ln(Y_1)}$	$\overline{\ln(Y_3)}$	t*	t(0.975,16)	Comment
PFAVE	0.983311	0.984249	0.209142	2.120	Not Diff.
DC60	-3.104553	-3.141833	0.219665	2.120	Not Diff.
F1/2	-5.070342	-5.264171	1.084849	2.120	Not Diff.
F2/2	-5.423593	-5.402603	0.073190	2.120	Not Diff.
F3/2	-5.840606	-5.797130	0.158285	2.120	Not Diff.
F4/2	-6.940625	-6.762864	0.437173	2.120	Not Diff.
F5/2	-6.403719	-6.544794	0.364755	2.120	Not Diff.
FM/2	-5.644880	-5.723091	0.382118	2.120	Not Diff.

Table (18): Statistical comparison of the mean between "Optimal Robust" Maximum Performance (data set 1) and Maximum HCF Life Expectancy (data set 3) installation CFD results.

Response	S_1	S_3	F*	F(0.975,8,8)	Comment
PFAVE	0.009538	0.009453	1.067896	4.43	Not Diff.
DC60	0.430507	0.370320	1.123346	4.43	Not Diff.
F1/2	0.395277	0.419342	1.577729	4.43	Not Diff.
F2/2	0.595343	0.605094	1.021587	4.43	Not Diff.
F3/2	0.551444	0.576764	3.045711	4.43	Not Diff.
F4/2	0.936279	0.689089	2.133706	4.43	Not Diff.
F5/2	0.823936	0.798711	1.110372	4.43	Not Diff.
FM/2	0.386132	0.445898	1.104159	4.43	Not Diff.

Table (19): Statistical comparison of the standard deviation between "Optimal Robust" Maximum Performance (data set 1) and Maximum HCF Life Expectancy (data set 3) installation CFD results.

Response	$\overline{\ln(Y_2)}$	$\overline{\ln(Y_3)}$	t*	t(0.975,16)	Comment
PFAVE	0.984589	0.984249	0.071929	2.120	Not Diff.
DC60	-2.972547	-3.141833	1.088837	2.120	Not Diff.
F1/2	-4.957721	-5.264171	1.819320	2.120	Not Diff.
F2/2	-5.288741	-5.402603	0.391603	2.120	Not Diff.
F3/2	-5.799162	-5.797130	0.007148	2.120	Not Diff.
F4/2	-7.367960	-6.762864	1.414981	2.120	Not Diff.
F5/2	-6.475028	-6.544794	0.178357	2.120	Not Diff.
FM/2	-5.604631	-5.723091	0.550795	2.120	Not Diff.

Table (20): Statistical comparison of the mean between "Optimal Robust" Maximum Engine Stability (data set 2) and Maximum HCF Life Expectancy (data set 3) installation CFD results.

Response	S_2	S_3	F*	F(0.975,8,8)	Comment
PFAVE	0.010004	0.009453	1.120069	4.43	Not Diff.
DC60	0.283570	0.370320	1.705428	4.43	Not Diff.
F1/2	0.281970	0.419342	2.211722	4.43	Not Diff.
F2/2	0.628281	0.605094	1.186619	4.43	Not Diff.
F3/2	0.628052	0.576764	1.185756	4.43	Not Diff.
F4/2	1.082130	0.689089	2.466089	4.43	Not Diff.
F5/2	0.859715	0.798711	1.158589	4.43	Not Diff.
FM/2	0.466342	0.445898	1.093797	4.43	Not Diff.

Table (21): Statistical comparison of the standard deviation between "Optimal Robust" Maximum Engine Stability (data set 2) and Maximum HCF Life Expectancy (data set 3) installation CFD results.

Response	Mt	α (degs)	CFD	DOE	t	t*	Comments
PFAVE	0.30	0.0	0.99432	0.99522	2.10090	0.73005	Not Diff.
DC60			0.07512	0.05562	2.10090	0.54532	Not Diff.
F1/2			0.00587	0.00450	1.96942	0.55327	Not Diff.
F2/2			0.00288	0.00336	1.96917	0.28857	Not Diff.
F3/2			0.00117	0.00123	1.91931	0.83415	Not Diff.
F4/2			0.00030	0.00018	1.96935	1.30110	Not Diff.
F5/2			0.00066	0.00038	1.96917	0.88946	Not Diff.
FM/2			0.00217	0.00193	1.96924	0.34888	Not Diff.
PFAVE	0.50	10.0	0.98835	0.98803	2.10090	0.27666	Not Diff.
DC60			0.04936	0.02052	2.10090	1.73825	Not Diff.
F1/2			0.00867	0.00729	1.96942	0.39272	Not Diff.
F2/2			0.00629	0.00311	1.96917	1.33491	Not Diff.
F3/2			0.00295	0.00317	1.91931	1.47962	Not Diff.
F4/2			0.00057	0.00114	1.96935	1.72954	Not Diff.
F5/2			0.00124	0.00116	1.96917	0.10854	Not Diff.
FM/2			0.00394	0.00317	1.96924	0.77457	Not Diff.
PFAVE	0.70	20.0	0.96629	0.96575	2.10090	0.43803	Not Diff.
DC60			0.04824	0.06511	2.10090	0.54417	Not Diff.
F1/2			0.00634	0.00363	1.96942	1.32794	Not Diff.
F2/2			0.00190	0.00401	1.96917	1.41370	Not Diff.
F3/2			0.00431	0.00671	1.91931	7.28503	Diff.
F4/2			0.00473	0.00192	1.96935	2.27527	Diff.
F5/2			0.00777	0.00352	1.96917	1.26278	Not Diff.
FM/2			0.00501	0.00397	1.96924	0.50478	Not Diff.

Table (22): Statistical comparison between CFD analysis and DOE prediction for the "Optimal Robust" Maximum Performance mission installation design.

Response	Mt	α (degs)	CFD	DOE	t	t*	Comments
PFAVE	0.30	0.0	0.99871	0.99517	2.10090	2.06018	Not Diff.
DC60			0.07797	0.05595	2.10090	0.60221	Not Diff.
F1/2			0.00603	0.00507	1.96942	0.36478	Not Diff.
F2/2			0.00208	0.00360	1.96917	1.02288	Not Diff.
F3/2			0.00114	0.00127	1.91931	1.56370	Not Diff.
F4/2			0.00017	0.00016	1.96935	0.14723	Not Diff.
F5/2			0.00065	0.00046	1.96917	0.55175	Not Diff.
FM/2			0.00217	0.00211	1.96924	0.09142	Not Diff.
PFAVE	0.50	10.0	0.98835	0.98803	2.10090	0.27666	Not Diff.
DC60			0.05149	0.02049	2.10090	1.82491	Not Diff.
F1/2			0.00899	0.00764	1.96942	0.37888	Not Diff.
F2/2			0.00638	0.00309	1.96917	1.37007	Not Diff.
F3/2			0.00290	0.00319	1.91931	1.85829	Not Diff.
F4/2			0.00030	0.00132	1.96935	3.79089	Diff.
F5/2			0.00124	0.00136	1.96917	0.14981	Not Diff.
FM/2			0.00396	0.00332	1.96924	0.68769	Not Diff.
PFAVE	0.70	20.0	0.96619	0.96580	2.10090	0.31636	Not Diff.
DC60			0.04643	0.06454	2.10090	0.59760	Not Diff.
F1/2			0.00571	0.00353	1.96942	1.17945	Not Diff.
F2/2			0.00304	0.00371	1.96917	0.37769	Not Diff.
F3/2			0.00557	0.00668	1.91931	3.27779	Diff.
F4/2			0.00491	0.00277	1.96935	1.47449	Not Diff.
F5/2			0.00738	0.00399	1.96917	0.97422	Not Diff.
FM/2			0.00532	0.00413	1.96924	0.59630	Not Diff.

Table (23): Statistical comparison between CFD analysis and DOE prediction for the "Optimal Robust" Maximum Engine Stability mission installation design.

Response	Mt	α (degs)	CFD	DOE	t	t*	Comments
PFAVE	0.30	0.0	0.99470	0.99480	2.10090	0.08472	Not Diff.
DC60			0.06192	0.05192	2.10090	0.33963	Not Diff.
F1/2			0.00490	0.00075	1.96942	4.11884	Diff.
F2/2			0.00279	0.00238	1.96917	0.30153	Not Diff.
F3/2			0.00148	0.00137	1.91931	1.34198	Not Diff.
F4/2			0.00048	0.00025	1.96935	1.62933	Not Diff.
F5/2			0.00061	0.00022	1.96917	1.61994	Not Diff.
FM/2			0.00205	0.00093	1.96924	1.62058	Not Diff.
PFAVE	0.50	10.0	0.98864	0.98738	2.10090	1.12168	Not Diff.
DC60			0.03958	0.02416	2.10090	1.01040	Not Diff.
F1/2			0.00653	0.00182	1.96942	3.18509	Diff.
F2/2			0.00588	0.00337	1.96917	1.05658	Not Diff.
F3/2			0.00355	0.00351	1.91931	0.23523	Not Diff.
F4/2			0.00097	0.00113	1.96935	0.39917	Not Diff.
F5/2			0.00199	0.00081	1.96917	1.47013	Not Diff.
FM/2			0.00362	0.00213	1.96924	1.47694	Not Diff.
PFAVE	0.70	20.0	0.96591	0.96488	2.10090	0.87609	Not Diff.
DC60			0.07454	0.09673	2.10090	0.50252	Not Diff.
F1/2			0.01207	0.00135	1.96942	5.14994	Diff.
F2/2			0.00299	0.00668	1.96917	1.52274	Not Diff.
F3/2			0.00231	0.00747	1.91931	3.54417	Diff.
F4/2			0.00331	0.00135	1.96935	1.91215	Not Diff.
F5/2			0.00586	0.00290	1.96917	1.13662	Not Diff.
FM/2			0.00531	0.00395	1.96924	0.68737	Not Diff.

Table (24): Statistical comparison between CFD analysis and DOE prediction for the "Optimal Robust" Maximum HCF Life Expectancy mission installation design.

REPORT DOCUMENTATION PAGE

Form Approved
OMB No. 0704-0188

1. AGENCY USE ONLY (*Leave blank*)	2. REPORT DATE	3. REPORT TYPE AND DATES COVERED
	December 2002	Technical Memorandum

4. TITLE AND SUBTITLE

Management of Total Pressure Recovery, Distortion and High Cycle Fatigue in Compact Air Vehicle Inlets

5. FUNDING NUMBERS

WU–708–53–13–00

6. AUTHOR(S)

Bernhard H. Anderson, Henry D. Baust, and Johan Agrell

7. PERFORMING ORGANIZATION NAME(S) AND ADDRESS(ES)

National Aeronautics and Space Administration
John H. Glenn Research Center at Lewis Field
Cleveland, Ohio 44135–3191

8. PERFORMING ORGANIZATION REPORT NUMBER

E–13672

9. SPONSORING/MONITORING AGENCY NAME(S) AND ADDRESS(ES)

National Aeronautics and Space Administration
Washington, DC 20546–0001

10. SPONSORING/MONITORING AGENCY REPORT NUMBER

NASA TM—2002-212000

11. SUPPLEMENTARY NOTES

Bernhard H. Anderson, NASA Glenn Research Center; Henry D. Baust, Wright-Patterson Air Force Base, Dayton, Ohio 45433; and Johan Agrell, Swedish Defence Research Agency, Bromma, Sweden. Responsible person, Bernhard H. Anderson, organization code 5850, 216–433–5822.

12a. DISTRIBUTION/AVAILABILITY STATEMENT

Unclassified - Unlimited
Subject Category: 07 Distribution: Nonstandard

Available electronically at http://gltrs.grc.nasa.gov

This publication is available from the NASA Center for AeroSpace Information, 301–621–0390.

12b. DISTRIBUTION CODE

13. ABSTRACT ***(Maximum 200 words)***

It is the purpose of this study to demonstrate the viability and economy of Response Surface Methods (RSM) and Robustness Design Concepts (RDC) to arrive at micro-secondary flow control installation designs that maintain optimal inlet performance over a range of the mission variables. These statistical design concepts were used to investigate the robustness properties of "low unit strength" micro-effector installations. "Low unit strength" micro-effectors are micro-vanes set at very low angles-of-incidence with very long chord lengths. They were designed to influence the near wall inlet flow over an extended streamwise distance, and their advantage lies in low total pressure loss and high effectiveness in managing engine face distortion.

14. SUBJECT TERMS

Aerodynamics; Propulsion; Fluid dynamics

15. NUMBER OF PAGES

68

16. PRICE CODE

17. SECURITY CLASSIFICATION OF REPORT	18. SECURITY CLASSIFICATION OF THIS PAGE	19. SECURITY CLASSIFICATION OF ABSTRACT	20. LIMITATION OF ABSTRACT
Unclassified	Unclassified	Unclassified	